DESIGN OPTIMIZATION OF HEADBAND FOR HEADPHONE

By

JASON LIN

A thesis submitted in partial fulfillment of
the requirements for the degree of

Master of Science in Mechanical Engineering

WASHINGTON STATE UNIVERSITY
School of Engineering and Computer Science

DECEMBER 2009

To the Faculty of Washington State University:

The members of the Committee appointed to examine the thesis of JASON LIN find it satisfactory and recommend that it be accepted.

_____

Dave (Dae-Wook) Kim , Ph.D., Chair

_____

Hakan Gurocak, Ph.D.,

_____

Linda (Xiaolin) Chen, Ph.D.,

ACKNOWLEDGMENT

I am sincerely thankful to Dr. Dave Kim, whose encouragement, instruction and support from topic initiation to the final research result enabled me to develop a truly professional understanding of this subject. I benefited greatly from the knowledge and wisdom of Dr. Kim, and I feel privileged to have studied under his guidance. In addition to being a great professor, he was a wonderful person, and a true gentleman, whose warm personality and enthusiasm have had a profound influence on my life.

Lastly, I offer my thanks to Dr. Linda Chen whose instruction for FEA and James Reamer and John Hyder who assisted me while conducting experiments

DESIGN OPTIMIZATION OF HEADBAND FOR HEADPHONE

ABSTRACT

by Jason Lin, M.S.
Washington State University
December 2009

Chair: Dae-Wook (Dave) Kim

There is an ever increasing demand for improvement of performance, reliability and cost effectiveness of headphones. A product designer is required to integrate the perspectives from marketing, consumers and manufacturing by using efficient analysis tools which can be applied into a systematic approach to the problem.

The potential failure mode and effect analysis (FMEA) of headband design allows a designer to construct a qualitative analysis of a system for the purpose of identifying critical characteristics. It further allows the designer to examine the causes and effects associated with each potential failure mode's occurrence. Two high risk failure modes are improper clamping force and headband fatigue failure. Both failure modes are dominated by two design factors, metal band thickness and tensile strength. Finite Element Analysis (FEA) was used to estimate the design responses, which are headband fatigue life and clamping force. These responses coupled with the optimization module presented a solution which will help determine optimal metal band thickness and tensile strength, while maintaining the targets of performance; cost and reliability of the headband.

TABLE OF CONTENT

PAGE

LIST OF TABLES

PAGE

LIST OF FIGURES

PAGE

CHAPTER 1

INTRODUCTION

Headphones can be defined as small speaker units that can be retained close to a listener's ears. They also provide a means of connecting to a stereophonic, monophonic, or binaural audio-frequency signal source such as a stereo, radio, CD player, or PC. Headphones allow users to hear reproduced sounds without disturbing people in their vicinity and can be carried conveniently or placed atop the head for hands free use. Special headphones also function to protect the user’s ears by isolating loud outside noises. To extend the application of headphones, a headset is used which is an integration of a headphone and a microphone and can be used for two-way communication.

Mechanically, headphones are constructed with a pair of small speakers, or less commonly a single speaker, with a headband. A headband is one type of component to hold the ear cups close to a user's ears. The ear pads are an interface between the headphones and the human body. The pads consist of a filing material, around which is formed of flexible elastic plastic having high elasticity to help distribute force and provide comfort.

There are two conventional headband structures commonly used; Over-the-head and Behind-the-head. For an Over-the-head style (Figure 1.1 (a)), the speaker systems are installed on both ends of a headband which is formed to fit the top of the users head. The load of the speaker units is evenly distributed throughout various portions of human head by the headband. The headband creates clamping force to secure the device on the head, and provides a better sealing on the ear pads for improved acoustic and security purposes. For a Behind-the-head style (Figure 1.1 (b)) headphone, the headband is formed to enclose the rear of user’s head. Therefore, no load is applied to the top of the user’s head by the headband. This type of headphone can add a clamping force to the user’s temples

however. No matter which style of headband is chosen, the load on the users head should be properly distributed or minimized so that listeners can wear the headphones without feeling too much weight or pressure. Thus, the design of the headphones should allow listeners to comfortably and conveniently wear the headphones for an extended period of time.

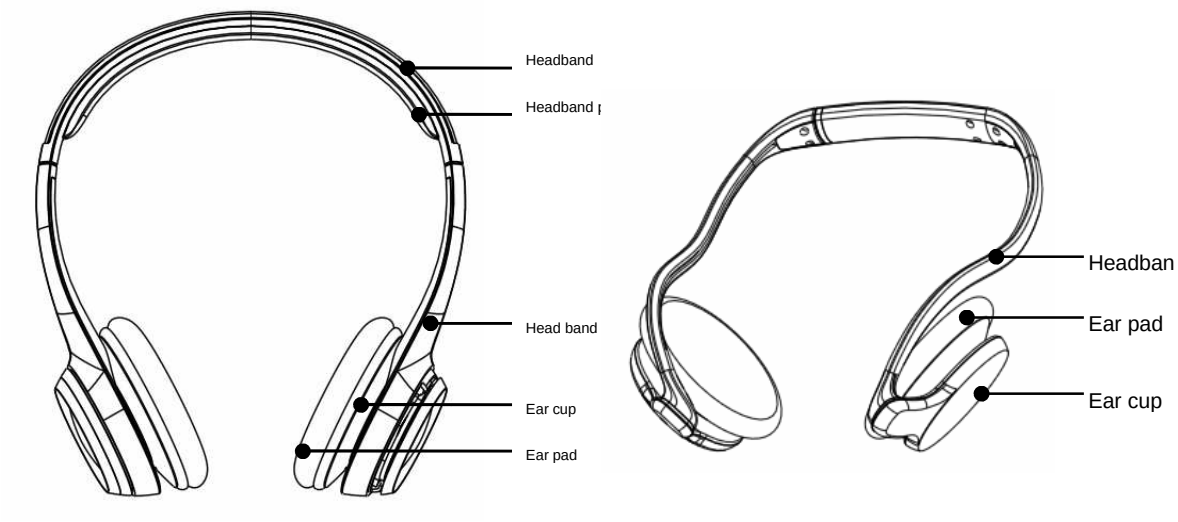

(a) Over-the-head style (b) Behind-the-head style

Figure 1.1: Headphone basic structures

When it comes to the design of the mechanical systems of a headphone, the headband is the major component that bridges the speakers and securely attaches the phone to the user. Some innovative designers have tried to improve the ergonomic fit of the headphones by adding supports on the neck or the shoulder. However few of these designs have been successfully applied in industry so far. For example, a neck support structure (Figure 1.2) invented by Lee Y. has the potential to improve aesthetics and ease of use of the headphones making them more marketable.

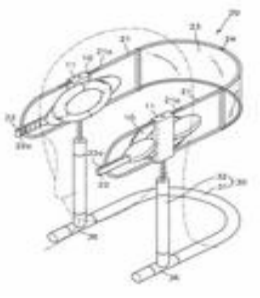

Figure 1.2: Headphone shoulder support structures [1]

To achieve comfort and acoustic performance purposes, it is essential to design a headband that will fit as many users' heads as possible. By adding adjustable mechanisms on the headband, the headphone can fit a wider range of head sizes and shapes. The headphones flexible headband can also be tensioned so that the listener's various movements, such as turning or shaking will not make the headphone come loose. Besides the ergonomic considerations, the reliability and durability of the headband are always an issue and remain the key consideration in design. Mechanical failure of headbands has often been observed because of frequent bends and twists made by the users. Headbands under these cyclic loadings were failed due to fatigue at the high stress concentration area. Moreover, headbands can be exposed to large deformations during extremely rigorous usage, which can cause local damage or permanent deformation of headband. Figure 1.3 (a) and (b) show the basic structure of the over-the head type headband, which consists of the metal band, the headband pad and the cable. The functions of each headband component are shown in Figure 1.4.

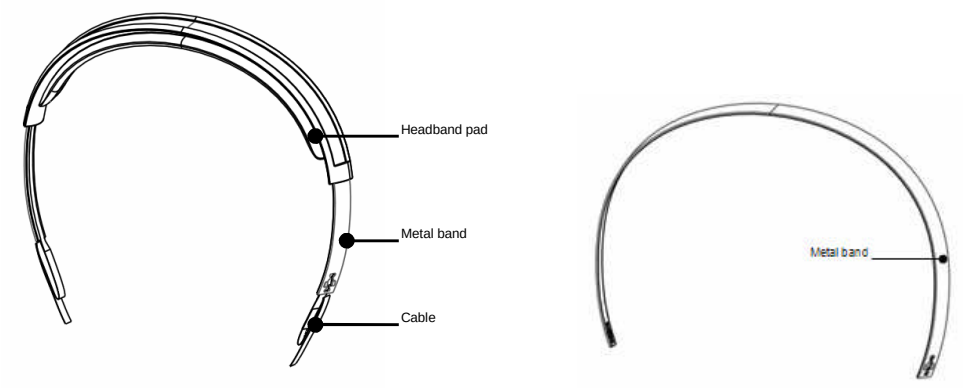

(a) Overall structure (b) Metal band

Figure 1.3: Headband basic structures

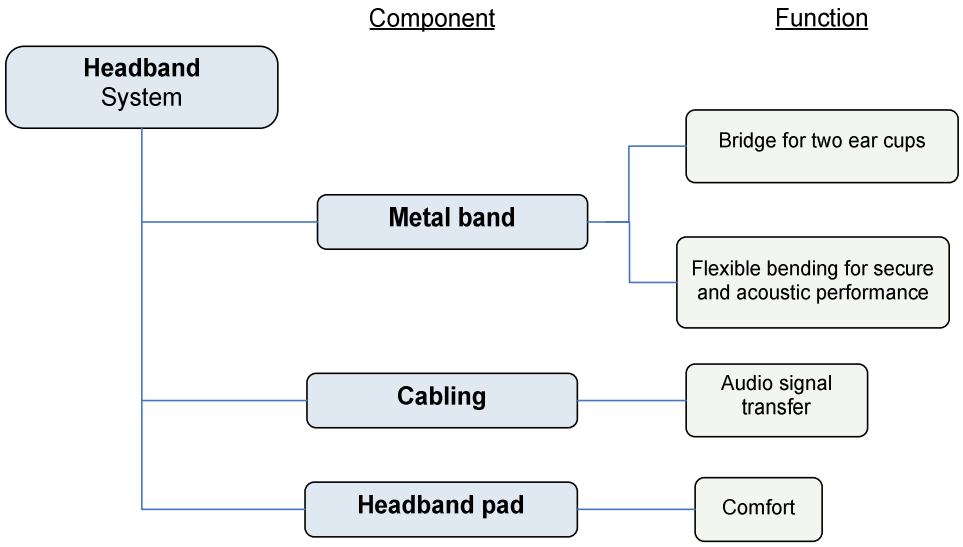

Figure 1.4: Headband components function

This study aims to develop the design methodology, which integrates design problem identification, failure mode effect and analysis, fatigue failure analysis, and design optimization for headband design. This particular study will also show how the metallic headband can be designed to prevent mechanical failures, meet ergonomic requirements, and reduce overall costs.

This thesis is composed of 6 chapters. Chapter 1, introduction, provides some general information about the headphone, its structures, and the design requirements. The Literature Review, Chapter 2, provides additional depth regarding topics significant to the direction of this report and provides details of past and present research in relevant areas. Chapter 3, the objectives, concisely explains the reason for this research and the goals that were established at the onset of this study. Chapter 4 informs the reader of the procedures and equipment used during all numerical, experimental, and analytical analysis in this work. Next, Chapter 5 presents the results obtained from the experimental work and also provides a discussion of these results. Finally, Chapter 6 establishes conclusions from this study and recommends future study topics.

CHAPTER 2

LITERATURE SURVEY

In this chapter, the design tools used in this study will be introduced. Some fundamental knowledge is involved early in the product development cycle to ensure the performance and quality requirements for the headphones are met. In addition, the recent research outcomes provided by the design tools used in this study will be presented.

2.1 Failure Mode and Effects Analysis (FMEA)

Customers are placing increased demands on companies to provide high quality, reliable headphones. The increasing capabilities and functionality of headphones are making it more difficult for manufacturers to maintain quality and reliability while meeting cost goals. Traditionally, reliability has been achieved through extensive testing and use of techniques such as probabilistic reliability modeling. However, these are techniques performed in the late stages of development. Often, it is challenge to consider product quality and reliability early in the product development cycle. Failure Modes and Effects Analysis (FMEA) is a methodology for analyzing potential reliability problems early in the product development cycle. This makes it easy to take action that will overcome any development issues, thereby enhancing reliability through product design.

There are several types of FMEA, but careful consideration must be made before selecting the correct analysis for a given situation. FMEA should always be performed when failure would mean potential harm or injury to the user of the end item being designed. The types of FMEA include system, design, process, service, and software. In this study, design FMEA was used to identify possible failure problems during the headphones design phase.

The process for conducting a design FMEA is pretty straightforward. The basic steps are outlined below. The analysis is recorded as Table 2.1.1.

1. Review the design – Use a blueprint or schematic of the design/product to identify each component and interface.
2. Brainstorm potential failure modes – Identify Failure Modes. A failure mode is defined as the manner in which a component, subsystem, system, process, etc. could potentially fail to meet the design intent.
3. List potential effects of failure – There may be more than one for each failure.

Table 2.1.1: Example of FMEA form

System	LTN2001 GPS SSU	Potential Failure Mode and Effects Analysis (Design FMEA)									Revision	B			
Subsystem	Receiver Card										Prepared By	Robert Crow			
Part Number	468230-100										FMEA Date	8/18/1992			
Design Lead	J. Davies										Revision Date				

Item / Function	Potential Failure Mode(s)	Potential Effect(s) of Failure	Sev	Potential Cause(s)/ Mechanism(s) of Failure	Prob	Current Design Controls	Det	RPN	Recommended Action(s)	Responsibility & Target Completion Date	Action Results: Actions Taken	New Sev	New Occ	New Det	New RPN
Circuit Block 4.1.1	Output loss from pre-amp	Receiver & output data loss; track loss; GPS shut-down	5	C1 short	1	PR-20 & HW-5	2	10	QA Proc 20-6	R. Jones, 11/30/92	Added to control plan	2	1	1	2
			5	C88 short	2		2	20	QA Proc 20-6	R. Jones, 11/30/92	Added to control plan	2	1	1	2
			5	L1 open/short	3		2	30	QA Proc 20-3	R. Jones, 11/30/92	Added to control plan	2	2	1	4
			5	U21 function	4		2	40	Test 147	R. Jones, 11/30/92	Added to control plan	2	3	1	6
								0							0
Circuit Block 4.1.2	Undetected & insignificant component failure mode	No noticeable system effect	1	C1open/chg val.	2	None	8	16	None						0
			1	C88open/chg val	2		8	16	None						0
								0							0
Circuit Block 4.2.1	Loss of signal from 2nd RF amplifier & 1st down converter	Loss of position, velocity & time output data; track loss; GPS shut-down	4	C2 short	1	PR-20 & HW-5	2	8	QA Proc 20-6	D. Howell 10/15/92	Added to control plan				0
			4	C3 short	1	PR-20 & HW-5	2	8	QA Proc 20-6	D. Howell 10/15/92	Added to control plan	2	1	1	2
			4	C4 open/short	2	PR-20 & HW-5	2	16	QA Proc 20-6	D. Howell 10/15/92	Added to control plan	2	1	1	2
			4	C5 short	2	PR-20 & HW-5	2	16	QA Proc 20-6	D. Howell 10/15/92	Added to control plan	2	1	1	2
			4	C66 open/short	2	PR-20 & HW-5	2	16	QA Proc 20-6	D. Howell 10/15/92	Added to control plan	2	1	1	2
			4	C99 short	3	PR-20 & HW-5	2	24	QA Proc 20-6	D. Howell 10/15/92	Added to control plan	2	2	1	4
			4	FL1 short/open	5	None	2	40	100% Insp.	D. Howell 10/15/92	Added to control plan	2	2	2	8
			4	FL2 short/open	5	None	2	40	100% Insp.	D. Howell 10/15/92	Added to control plan	2	2	2	8
			4	R2open/chg val	2		2	16	None						0
			4	R18 open/chg val	2		2	16	None						0

4. Assign Severity rankings – Based on the severity of the consequences of failure.
5. Assign Occurrence rankings – Based on how frequently the cause of the failure is likely to occur.
6. Assign Detection rankings – Based on the chances the failure will be detected prior to the customer finding it.
7. Calculate the RPN – Severity x Occurrence x Detection.
8. Develop the action plan – Define who will do what by when.
9. Take action – Implement the improvements identified by your DFMEA team.
10. Calculate the resulting RPN – Re-evaluate each of the potential failures once improvements have been made and determine their impact on the RPNs.

Failure Modes and Effects Analysis (FMEA) is a design tool that mitigates risks measured in terms of Risk Priority Number (RPN). RPN is a product of occurrence, severity, and detection difficulty. Measuring severity and detection difficulty is very subjective and offers no universal scale so it can be very inconsistent. RPN is also a product of ordinal variables, which is not meaningful as a proper measure. To solve those shortcomings, Seung J. Rhee and Kosuke Ishii introduced a new methodology called Life Cost-Based FMEA [2]. LCB-FMEA measures risk in terms of cost. Cost is a universal language that can be easily understood in terms of severity among engineers and others. Thus, failure cost can be estimated using the following simplest form:

$$\text{Expected failure cost} = \sum_{i=1}^{n} p_i c_i$$

p: probability of a particular failure occurring,

c: cost associated with that particular failure

In additional to the RPN being poorly defined, FMEA has pitfalls regarding time requirements, failure to identify key errors, and the fact that it is performed too late in the design process. Lawrence P. Chao and Kosuke Ishii developed error-proofing methods for the product development process [3]. These methods help prevent serious design errors that can compromise project features, time to market, or cost to assist FMEA. The method decomposes the design process into six potential problem areas—knowledge, analysis, communication, execution, change, and organization errors—with a question-based FMEA approach. Table 2.1.2 shows the design error classification system. This system can help designers build sets of questions which may assist in error location processes.

Table 2.1.2: Design error classification system categories [3]

Category	Description
Knowledge	Inexperience or misunderstanding of the system
Analysis	Inaccurate assessment of the system
Communication	Mistransfer or misinterpretation of information
Execution	Improper or inaccurate implementation
Change	Unanticipated variation or modification
Organization	System or managerial deficiencies

FMEA is a knowledge-base driven analysis method, which requires a designer to have a broad and deep expertise of searching for, and reusing, archived design knowledge. The function-failure design method (FFDM) [4] provides designers a methodology for performing failure analysis in conceptual design and also aids them by using a function-based concept generator approach [5] to streamline the design process. To extend the research for FFDM, Robert B. Stone explored an approach to populating a knowledge base with actual failure occurrence historical information. The function-failure (EF) matrix is generated by multiplying the function-component (EC) and component failure

(CF) together [6]. EC, CF and EF are matrixes. The EF matrix relates historical failure occurrences to functionality and is used as the knowledge base in the FFDM approach. Results indicate that encoding failure data using more detailed functional models allows for a more robust knowledge base.

Most FMEA research focuses on improving traditional FMEA limitations by using different measurement schemes, considering multiple failure scenarios, and incorporating sensitivity analysis. To enhance FMEA analysis and improve the reliability in the design, G. Arcidiacono and G. Campatelli developed an approach called failure mode and effect tree analysis (FMETA) [7] which uses the support of the AD methodology combined with FMEA and FTA. FMETA allows the designer to find the most critical characteristic of the product from a reliability point of view and provides the designer with a set of possible changes. A scheme of the FMETA is presented in Figure 2.1.1

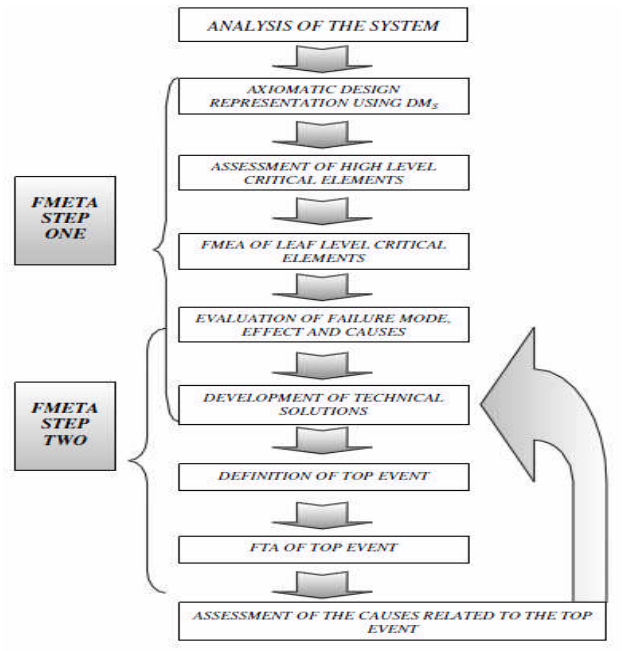

Figure 2.1.1: Scheme of the FMETA approach [7]

2.2 Effect of headband clamping force

The clamping force of the headband drives the headphones functional performance which is defined by comfort, control of sound energy, attenuation, and wearing security. Most related research focuses on hearing protection devices. However, the headphone and hearing protector have very similar design parameters for the headband even though some of their design targets are uncommon. For example, hearing protectors have much higher clamping requirements than the standard headphone.

The control of attenuation in a headphone depends on the design and the materials used in various elements of the assembly, such as: ear cup, foam lining and headband force. Paulo Henrique Trombetta Zannin [8] experimentally evaluated the effect of headband force on the noise attenuation of a circumaural hearing protector. The result shows that a reduction of the contact force between the cushion and the head produces a leak in sound energy to the ear. Increasing the contact force eliminates part of the sound energy leak to the inside of the cup in the low frequency range. As the headband force increases to a maximal deformation of the cushion, attenuation reaches 20 dB at 200 Hz (Figure 2.2.1). Increasing the headband force is a limiting factor to the use of the earmuff however, as it becomes uncomfortable at a high level of pressure. In real work environments, users will try to diminish this force making the protector more comfortable, but also forcing the headband outwards.

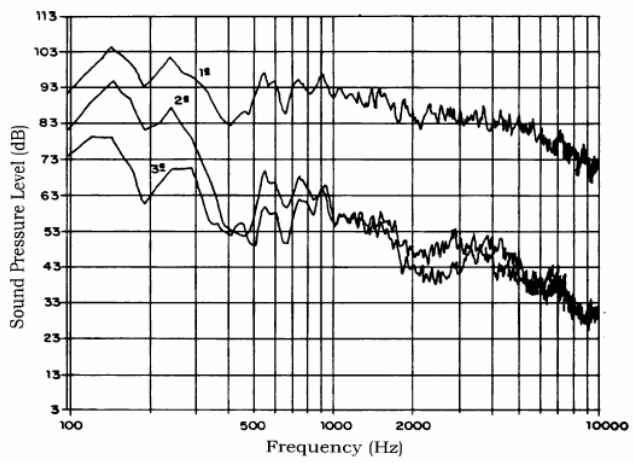

Fig. 2.2.1: Attenuation obtained with variation in the contact force: 1st curve: sound pressure level measured without the earmuff, 2nd curve: sound pressure level measured using the earmuff, 3rd curve: sound pressure level measured with total deformation of the cushion. [8]

It seems to always become a question of how to measure the comfort level for the end user based on the headband clamping force. Because “comfort” is subjective and difficult to quantify, some pressure mapping methods have been developed for the footwear industry to assist in predicating appropriate comfort levels [9]. For the headphone, a subjective test is still the mainstream method for measuring comfort. Yeh-Liang H introduced the comfort indices for hearing protection. By using the “comfort tester” (Figure 2.2.2), He concluded that for earmuffs, soundproofing is the most important factor, followed by air tightness, weight, heat-sinking ability, texture, and finally headband force [10]. The headband force is measured conforming to EN352-1 (1993), using a standard head frame with an s-shape load cell in the center of the tester Figure 2.2.2. When an earmuff is mounted on the two side plates, the load cell can measure the pressure applied by the earmuff. The height of the head frame and the distance between the two side plates can be adjusted for measuring the headband forces for different head sizes.

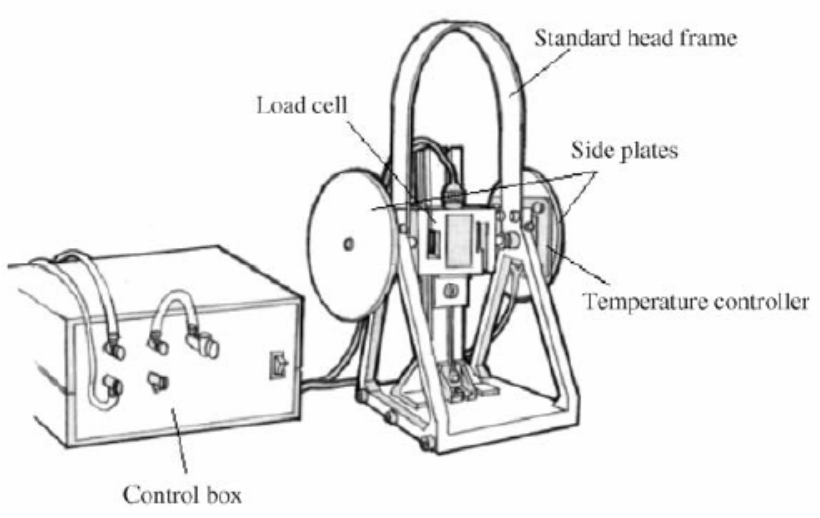

Figure 2.2.2: The earmuff ‘‘comfort tester’’ [10]

The test result in the Table 2.2.1 shows that for the same earmuff, air-tightness has strong correlation with the headband force. Air-tightness, and therefore soundproofing effect, may be affected when trying to reduce headband force. For the subjects' perception of earmuff headband force, Figure 2.2.3 shows continuous contours of the relation of subjects' perceived feelings and magnitudes of earmuff headband force. Further interpolating the data, it was found that a headband force under 10.5N would be described by 80% of wearers as ‘‘no particular feeling’’ or ‘‘a little tight’’.

Tanle 2.2.1: Correlation between airtightness and headband force for the same earmuff [10]

Headband force (N)	Earmuff A	Earmuff B
	Airtightness (%)	
6	91.8	91.0
8	92.6	92.2
10	92.8	94.2
12	93.3	95.5
14	96.4	98.0
Pearson coefficient	0.88	0.99

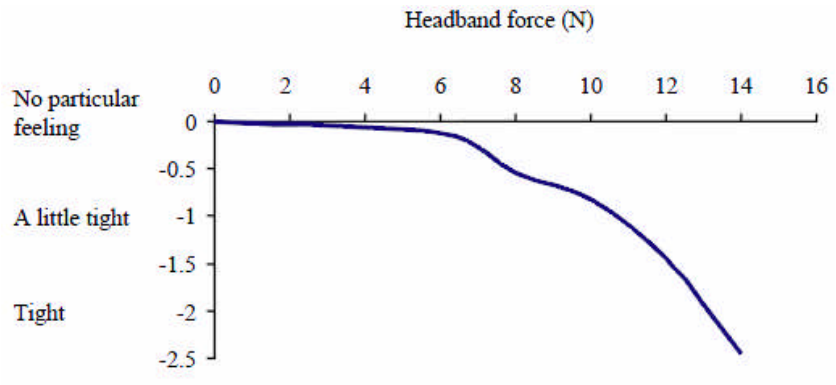

. **Figure 2.2.3: Relation of subjects' perceptions and magnitudes of earmuff headband force and weight. [10]**

The proper clamping force of the headband is important to obtain comfort and provide an adequate acoustic isolation. Both are indispensable functional performance objectives, and need to be optimized for maximum gains. To define the ideal clamping force, a subjective test can be conducted as long as care is used while designing the questionnaire. The different applications of headband use may have different weights for criteria during the optimization process. For most tests however, comfort has higher weight than acoustic performance or wearing security.

2.3 Fatigue design theories and the applications

Fatigue can be defined as the progressive and localized structural damage that occurs when a material is subjected to cyclic loadings, even if the applied stresses are lower than the material's yield point. Since fatigue has been found to be one of the major failure modes in metal products, dependable design and analysis against fatigue failure have been implemented into most product designs. Two primary fatigue design methods are usual to predicate the fatigue life: the stress-life approach and the strain –life approach. Both design methods have their own region of application with some degree of overlap between them. It is insight gained from the understanding both approaches which allows the designer to choose the method or methods that are most appropriate for the problem at hand.

2.3.1 Stress-Life Method

The stress-life (S-N) approach is still widely used in design applications where the applied stress is primarily within the elastic range of material, and the resultant life (cycle to failure) is long. The basis of the S-N method is the Wohler S-N diagram, shown schematically for two materials in Figure 2.3.1. The S-N diagram plots nominal stress amplitude S versus cycles to failure N. There are numerous testing procedures to generate the required data for a proper S-N diagram. S-N test data are usually displayed on a log-log plot, with the actual S-N line representing the mean of the data from several tests.

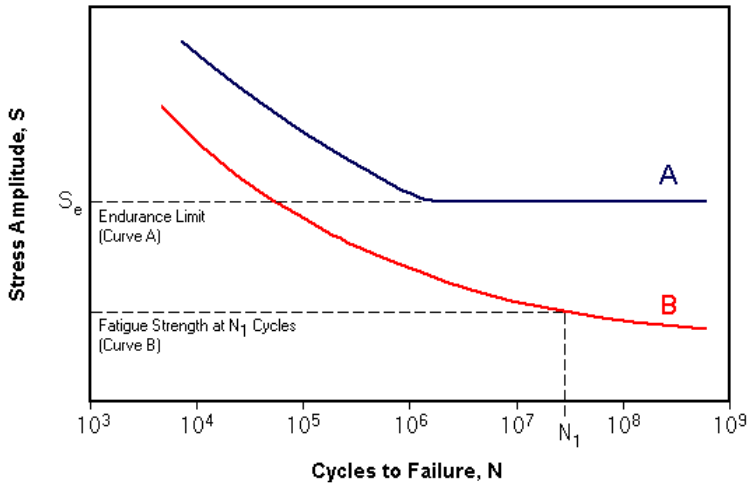

Figure 2.3.1: Typical S-N Curves

Certain materials have a fatigue limit or *endurance limit* that represents a stress level below which the material does not fail and can be cycled infinitely. If the applied stress level is below the endurance limit of the material, the structure is said to have an *infinite life*. This is characteristic of steel and titanium in benign environmental conditions. A typical S-N curve corresponding to this type of material is displayed by Curve A in Figure 2.3.1. Many non-ferrous metals and alloys, such as aluminum, magnesium, and copper, do not exhibit well-defined endurance limits. These materials instead display a continuously decreasing S-N response, similar to Cuve B in Figure 2.3.1. In such cases a fatigue strength S_f for a given number of cycles must be specified. An effective endurance limit for these materials is sometimes defined as the stress that causes failure at $1x10^8$ or $5x10^8$ loading cycles.

Several empirical relationships that relate alternating stress to mean stress have been developed to address this difficulty. These methods define various curves to connect the endurance limit, on the alternating stress axis, to either the yield strength, S_y, ultimate

strength S_u, or true fracture stress σ_f on the mean stress axis. The following relations are available in the Stress-Life module:

Goodman (England, 1899):

$$\frac{S_a}{S_e} + \frac{S_m}{S_u} = 1 \quad (2.1)$$

Gerber (Germany, 1874):

$$\frac{S_a}{S_e} + \left(\frac{S_m}{S_u}\right)^2 = 1 \quad (2.2)$$

Soderberg (USA, 1930):

$$\frac{S_a}{S_e} + \frac{S_m}{Sy} = 1 \quad (2.3)$$

Morrow (USA, 1960s):

$$\frac{S_a}{S_e} + \frac{S_m}{\sigma_f} = 1 \quad (2.4)$$

A graphical comparison of these equations is shown in Figure 2.3.2. The two most widely accepted methods are those of Goodman and Gerber. Experience has shown that test data tends to fall between the Goodman and Gerber curves. Goodman is often used due to mathematical simplicity and slightly conservative values.

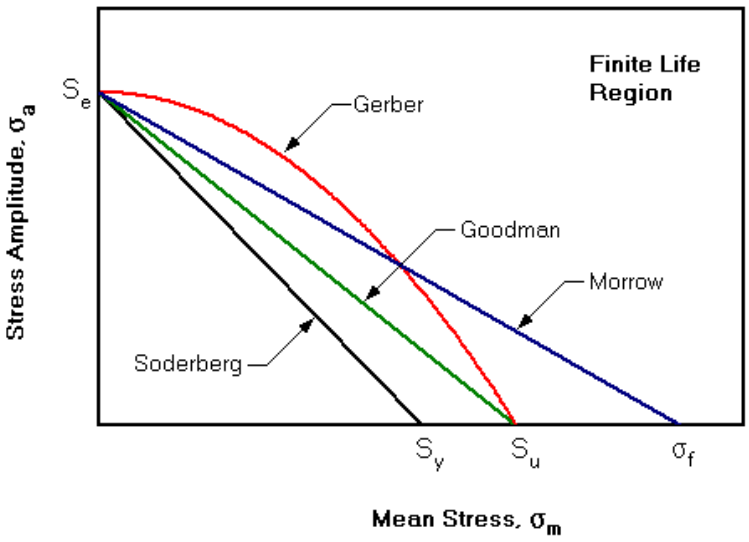

Figure 2.3.2: Comparisons of Mean Stress Equations

The stress –life method is not often used in product design because this approach does not work well in low-cycle applications where the applied strains have a significant plastic component. In this range the strain-based approach is much more appropriate. The dividing line between low and high cycle fatigue depends on the material being considered, but usually falls between 10 and 10^5 cycles. Some studies have applied the stress- life method with reasonable accuracy. S. Kwofie proposed a stress-based moel for correlating data and predicting fatigue life under conditions where cyclic creep–fatigue interaction occurs [11]. This model is an extension of the Basquin's stress–life relation[12] and considers that both the fatigue strength coefficient and fatigue strength exponent are sensitive to mean stress. This also requires that both decrease as an exponential function of the ratio of mean stress-to-stress amplitude. To extend the research of mean stress on the fatigue strength and life, S. Kwofie presented a function of the ratio of mean stress to the ultimate tensile strength. $\sigma_f = f(\sigma_m / \sigma_u)$ .The severity of

damage depends on the relative measure of mean stress to the ultimate tensile strength of the material. The proposed relationship between fatigue strength and mean stress is non-linear and reflects the true shape or characteristics of the conventional stress/strain–life curves, and has applications in both low-cycle and high cycle fatigue regimes. S. Kwofie's model and the strain-based Smith–Watson–Topper (SWT) model are compared with experimental data in Kwofie's paper. He then concludes that the strength and life prediction capability of the present approach is an improvement to stress-based methods, and has been shown to be superior to the popular SWT strain-based approach [13].

Another study of mean stress effect for the fatigue limit related to tensile strength had been done by Rune Johansson and Hans Nordberg. In Fig 2.3.3 the fatigue limit is related to the static strength for temper rolled strips of 1.4310 (AISI 301) in the 800 to 1700 MPa strength range. The fatigue limit (Se) is increased to a tensile strength (S_u) of 1500 MPa and then levels off. This data also indicates that the fatigue ratio, Se/ S_u, being approximately 0.35 at a stress ratio (R) ≈ 0 which is typical for austenitics, remains unchanged up to S_u ~1500 MPa. [14]

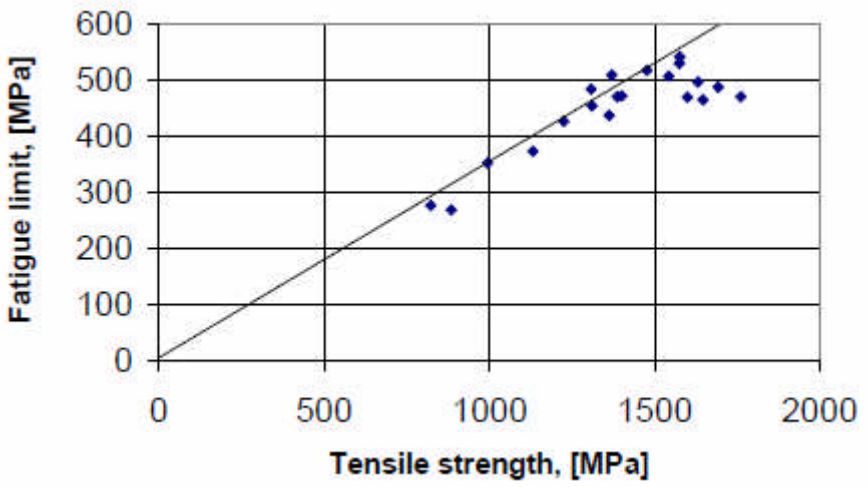

Fig. 2.3.3: Fatigue limit for the austenitic stainless steel l, 1.4310 (301), cold worked to different strength levels. R = 0. Thickness 0.15 – 0.8 mm. The 0.35 slope is indicated [14].

2.3.2 Strain- Life

The strain-life method is based on the observation that in many components the response of the material in critical locations is strain or deformation dependent. When load levels are low, stresses and strains are linearly related. Consequently, in this range, load-controlled and strain controlled test results are equivalent. For high loading levels, in the low cycle fatigue regime, the cyclic stress-strain response and material behavior are best modeled under strain-controlled conditions. Early fatigue research showed that damage is dependent on plastic deformation or strain in the material. In 1910, Basquin observed that Stress-Life data could be modeled using a power relationship, which results in a straight line on a log-log plot. This observation corresponds to elastic material behavior in the Strain-Life approach. The Basquin equation can be expressed in terms of true elastic strain amplitude as [12]:

$$\varepsilon_e = \frac{\sigma_a}{E} = \frac{\sigma'_f}{E}(2N_f)^b \quad (2.5)$$

where: ε_e is the elastic component of the cyclic strain amplitude

σ_a is the cyclic stress amplitude

σ'_f is the regression intercept called the *fatigue strength coefficient*

N_f is the number of cycles to failure

b is the regression slope called the *fatigue strength exponent*

In the 1950's Coffin and Manson independently found that plastic Strain-Life data could also be modeled using a power relationship:

$$\varepsilon_p = \varepsilon'_f(2N_f)^c \quad (2.6)$$

where: ε_p is the plastic component of the cyclic strain amplitude

ε'_f is the regression intercept called the *fatigue ductility coefficient*

N_f is the number of cycles to failure

c is the regression slope called the *fatigue ductility exponent*

The Strain-Life Curve can be formed by summing the elastic and plastic components:

$$\varepsilon_t = \varepsilon_e + \varepsilon_p \quad (2.7)$$

$$\varepsilon_t = \frac{\sigma_f^{'}}{E}(2N_f)^b + \varepsilon^{'}_f (2N_f)^c \quad (2.8)$$

This model only works when the mean stress is zero and the load is completely reversible. The influence of the elastic and plastic components on the strain-life curve is shown in Figure 2.3.4.

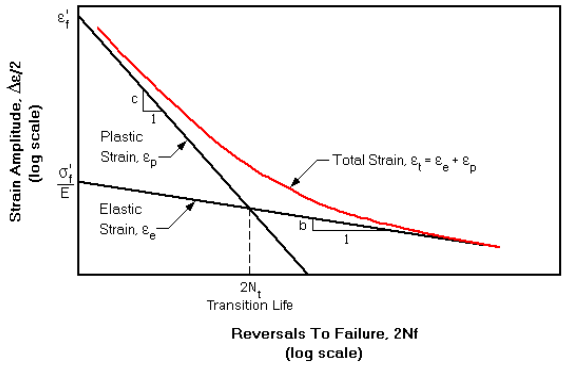

Figure 2.3.4: Typical Strain-Life Curve [15]

In terms of the strain-life relationship when the mean stresses are not zero, the *Morrow Mean Stress Correction* may be expressed as:

$$\varepsilon_t = \frac{\Delta\varepsilon}{2} = \frac{\sigma_f^{'} - \sigma_0}{E}(2N_f)^b + \varepsilon^{'}_f (2N_f)^c \quad (2.9)$$

where the mean stress σ_0 is positive for tensile stress and negative for compressive stress. A different method for modifying the strain-life curve to account for mean stress was proposed by Smith, Watson, and Topper. Their approach uses the Basquin relation relating the maximum stress σ_{max} of a fully-reversed cycle to fatigue life:

$$\sigma_{\max} = \sigma'_f (2N_f)^b \quad (2.10)$$

Multiplying the strain-life equation by this term gives the Smith-Watson-Topper (SWT) Mean Stress Correction:

$$\frac{\Delta\varepsilon_1}{2}\sigma_1^{\max} = \sigma_{f'}\varepsilon_f'(2N_f)^{b+c} + \frac{\sigma_f^2}{E}(2N_f)^{2b} \quad (2.11)$$

The SWT equation predicts that no fatigue damage occurs when the maximum stress is zero or negative (i.e., compressive), which is not always true. Therefore the Morrow correction should be used only for loading sequences that are predominantly compressive. The headband design is a case of predominant tensile loading; therefore, the SWT approach is more conservative than the Morrow approach and is thus recommended.

The stain-life equation Eq. (2.11) requires four empirical constants (b, c, σ_f', ε_f'), which may be approximated from monotonic prosperities. Mechanical properties determined from monotonic tensile tests are often used in the design of components. However, in service, most components experience cyclic loading and the fatigue properties of the materials are, therefore, of utmost importance to design engineers. Over the years, many researchers have attempted to develop correlations among the monotonic tensile data and fatigue properties of materials. Such correlations are desirable, considering the amount of time and effort required to obtain the fatigue properties, as

compared to the monotonic tensile properties. If reliable correlations with reasonable accuracy can be established, durability performance predictions and/or optimization analyses can be performed. This will substantially reduce time and cost associated with material fatigue testing.

The fatigue strength coefficient, σ_f', is analogous to the true fracture strength, σ_f, obtained from a tensile test. Several relations for estimating the fatigue strength coefficient from true fracture strength have been proposed. Although estimates range from 0.92 σ_f' to 1.15σ_f' which is a fairly large gap. M.L. Roessle and A. Fatemi have conducted research that shows relatively good linear least squares fits for the data, and can be represented by [16]:

$$\sigma_f' = 4.28HB + 225(MPa) \quad (2.12)$$

$$\sigma_f' = 1.04S_u + 345(MPa) \quad (2.13)$$

Their approach is called the direct hardness method. The approximation from the literature is shown in Fig. 2.3.5

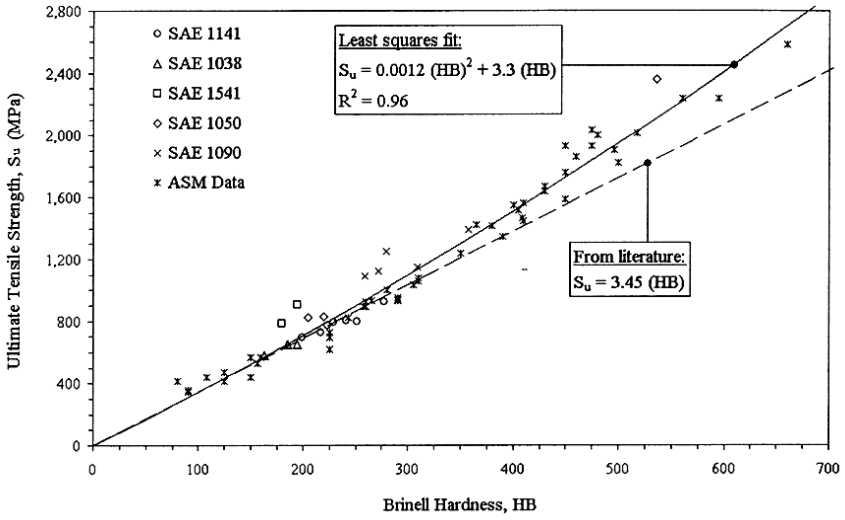

Figure 2.3.5: Ultimate Tensile Strength versus Brinell Hardness [16]

Indirect hardness methods utilizing the ultimate tensile strength predicted from hardness were proposed in Kwang-S's research. He then successfully applied his research to estimate fatigue properties for aluminum and titanium alloys. He concluded that:

(1) Roessle–Fatemi's (direct) hardness method can estimate fatigue properties very well for unalloyed and low-alloy steels and successfully for high-alloy steels. The method can be said to be very promising for steels.

(2) The so-called indirect hardness method utilizing Ba¨umel–Seeger's uniform material law or Maggiolaro–Castro's medians method with the predicted ultimate tensile strength from hardness was proposed. This is used to estimate fatigue properties for aluminum and titanium alloys, when the ultimate tensile strength is not available. The following relationship of ultimate tensile strength versus hardness was proposed for titanium alloys. **[**16]

$$\sigma_B = 3.61(HV) - 227 \quad \text{for} \quad \text{HV} > 100 \qquad (2.14)$$

Julie A. described the fatigue strength exponent b as varying from -0.05 to -0.12 for most metals with an average of -0.085. She also employed a fatigue ductility exponent, c. Here however, c is not well defined and as such, a rule-of-thumb approach must be followed rather than an empirical equation [15]. Coffin found c to be about -0.5. Manson found c to about -0.6. Morrow found that c varied between -0.5 and -0.7 **[**15**]**.

The fatigue ductility coefficient, ε_f' can be estimated using M.L. Roessle and A. Fatemi's model. A simpler second-order polynomial represents a very close agreement for $150 < HB < 700$ as follows:

$$\varepsilon'_f = \frac{0.32(HB)^2 - 487(HB) + 191000}{E} \qquad (2.15)$$

The fatigue strength exponent, *b*, with the average value of -0.09, and the fatigue ductility exponent, *c*, with the average value of -0.60 correspond well with Eq 2.11. This approximation uses only hardness and modulus of elasticity (in MPa) as inputs for strain–life approximation [15].

The strain-life approach has been used for product durability and reliability design as well. David J. observed that cyclic fatigue damage characteristics for simple loadings could be extended to multi-axial life prediction by strain-based theory for materials such as stainless 304. The SWT parameter (Eq. 2.11) has been employed to predict fatigue lives for both the in-phase and out-of-phase paths under investigation. The terms on the left hand side of the S.W.T equation (Eq. 2.11) are interpreted as the maximum principal strain amplitude and the maximum stress normal to that plane [17]

Yan-Hui Zhang and Stephen J. Maddox present the results of an investigation of the effect of weld toe burr grinding on the fatigue performance of non-load-carrying transverse fillet welded joints [18]. They used the strain life method to confirm the experimental results based on fracture mechanics. Their work suggested that the fatigue lives of the toe ground joints in this life regime were dominated by crack propagation processes. The fatigue life equation (Eq. 2.9) estimated by the Coffin-Manson equation, was modified by Morrow to take into account the local mean stresses being applied. To collect the fatigue properties, the hardness values of both the parent and weld metals were used to estimate the tensile strengths. These values were then used to estimate the low cycle fatigue properties of the parent and weld metals on the basis of the empirical relations suggested by Lawrence et al. [19], described below.

σ_{uts} = 3.45 HB

σ_y'=0.608σ_{uts}

b= 0.1667 log (2.1 + 917/ σ_{uts})

c =-0.7 < c < -0.5

n' =b/c

K' = σ_y'(0.002)$^{-n'}$

σ_f'= 0.95 σ_{uts} +370(MPa)

ε_f'= (σ_f'/ K')$^{1/ n'}$ (2-16)

2.4 Design optimization theories

To obtain the maximum benefit from available resources, optimization techniques must provide designers and decision makers the best possible vehicle for process control. The memory of past experiences, subconscious motives, incomplete logical processes, random selections and trial-and-error method are the basic ideas behind intuitive design in engineering. However, these thought processes do not tend to derive optimal design procedures or improve process efficiently. Oppositely, the optimal design can only be constructed by logical decision making and careful and concise preparation.

Designing products that operate satisfactorily under a wide variety of uncontrollable conditions, referred to as “noise,” is a design imperative. A product on which noise is a negligible effect, is referred to as a “robust” product—an inference made to the built-in immunity to noise [25]. Taguchi’s robust design methodology has been utilized to design quality and reliability into electronic circuits [20, 21]. The methodology aims at finding the settings of the design variables (DVs), which minimize or eliminate the effect of noise on state variables (SVs). In principle, this is achieved by exploiting the nonlinear relationship that may exist between design and state variables.

The optimum design is the best obtainable design given some predefined criteria. While working toward an optimum design, optimization routines employ three types of variables that characterize the design process: DV, SV, and the objective function.

DVs are usually geometric/model parameters such as length, thickness, diameter, or model coordinates. DVs are independent quantities that can be changed in order to achieve an optimum design. Upper and lower limits are specified to serve as “constraints”

on the design variables, but any value in the middle is fair ground. These limits define the range of variation for the DV.

SVs are response quantities that constrain the design. They are also known as "dependent variables," and are typically response quantities that are functions of the design variables. A SV may have a maximum and minimum limit, or it may be "single sided," having only one limit. The objective function is the quantity that is to be minimized or maximized. It should be a function of the DVs, that is, changing the values of the DVs should change the value of the objective function. These variables are then represented as scalar parameters. The independent variables in an optimization analysis are the design variables.

Often, there is more than one objective function to be optimized, or alternatively, the constraints which are required cannot be met by the current solution. Therefore, multiple objective optimization has been developed to optimize two or more conflicting objectives subject to certain SVs simultaneously. A multiple objective linear program is written as

"max" $\{\mathbf{C}\,\mathbf{x} = \mathbf{z} \mid \mathbf{x} \in S\}$ or "min" $\{\mathbf{C}\,\mathbf{x} = \mathbf{z} \mid \mathbf{x} \in S\}$ (2.18)

where **C** is the matrix of objective function coefficients, **x** is design variable vector, **z** is the objective function vector, and S is the dependable variable region [22].

Multiple objective optimization has been widely used in product design and development. Kim and Ramulu conducted a multiple objective optimization to design the drilling process for graphite-bismalemide/titanium stacks. A multiple objective linear program was used to optimize drilling feed and speed. This maximized the hole quality parameter while minimizing machining costs. Optimum process conditions for achieving the desired hole quality and process cost were found to be a combination of low feed and low speed when using carbide drills, and high feed and low speed in drilling with HSS-

Co drills. The sensitivity of weighting factors on the feasible process conditions depends on the optimal point position and distribution of each objective [23].

Identifying optimal parameters such as material properties and geometry conditions is easy when using optimization tools. The optimization for modeling structural fatigue failure, for example, is a quick and efficient design strategy. Mohammad Masum used DOE tools and procedures in his research for Design Optimization and Reliability of PWB Level Electronic Packages. Four model characteristics: printed wiring board (PWB) core in-plane Young's modulus, PWB core in-plane coefficient of thermal expansion, PWB core thickness, and the standoff solder joint height are chosen as the optimization inputs (design variables). These variables can then be altered to ensure high reliability and improved performance for the assembled product. The objective junction of the paper was to minimize average plastic work to improve the fatigue life of solder joints of the package. Sub-approximation, design of experiment and central composite design based response surface modeling methodologies are used to study the effects of each design variable on the fatigue life of the part [24].

The same approach was implemented by Tong H. in his thermo mechanical reliability research for flip-chip package assembly. The optimal design methodology was applied, by using a board-level high performance flip-chip ball grid array package assembly as the test vehicle. The method proved efficient for optimization of fatigue reliability of solder joints subjected to an accelerated thermal cycling test condition. Effects of different control factors, including solder composition, under fill, substrate size, lid thickness, stiffener ring width, test board size, solder mask opening on the substrate side, and pad size on the test board, are examined [25]

CHAPTER 3

OBJECTIVES

This resarch presents a discussion of the design methodology involved in the creation of a headband for use on headphones. To optimize the design it is imperative that the performance, quality and reliability of system compare well with cost effectiveness. The design methodology used in this study includes: failure mode effect analysis (FMEA) for problem identification, finite element analysis (FEA) for fatigue life estimation, and computational design of experiments (DOE) for design optimization. The detailed objectives follow:

1) Problem Identification

- Gather as much information as possible with regard to proper development / manufacturing processes, in order to avoid failures.
- Conduct FMEA to identify which failure modes will cause the greatest concerns to the designer or customer and that contain the highest risk priority numbers.
- Identify the actions needed to prevent the problems during the design phase.

2) Functional performance and reliability predication

- Conduct FEA to obtain the clamping force when the headband opens for the typical user.
- Conduct FEA to predict the stresses and strains which occur under loading conditions. An FEM allows detailed visualization of the positions where headband structures bend or twist and indicates the distribution of stresses or displacements.

- Conduct fatigue analysis using FEM to predict fatigue failure cycles under cyclic loadings.
- Verify the FEA results for the clamping force and fatigue life predictions and the stress-strain predictions, strain gages are used to measure the strain values for a headband.

3) Optimization method to integrate the system design

- Use the cost, headband clamping force and headband fatigue life as the input parameters for optimization.
- Use the multi-objective functions to optimize the headband parameters, which are the geometry and material of the headband.

Figure 3.1 shows the overall process flow to achieve these objectives.

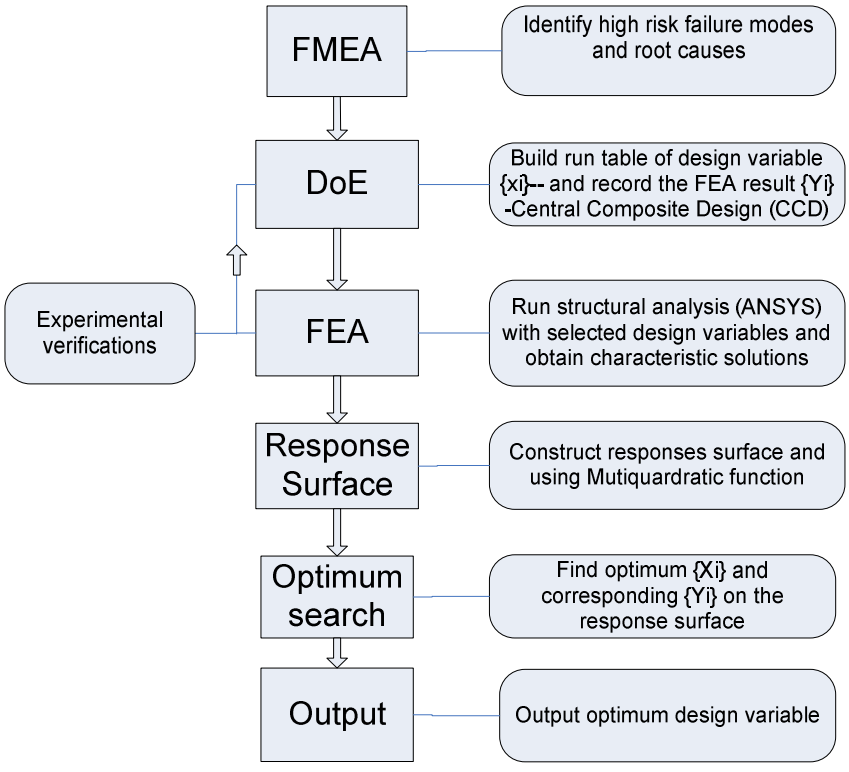

Figure3.1: Headband optimization flow using CCD based RS

CHAPTER 4

METHODS OF APPROACH

4.1 Failure Mode and Effect Analysis (FMEA)

A headband ensures that headphones can be secured on the user's head. It is also designed to connect the two ear cups while providing proper clamping force which will prevent sound energy leaks. Since the headband drives the major ergonomic and acoustic performance, a designer should spend much more time and resource during headband development, than in any other stage of manufacture. To lesson development time and prevent costly recalls or delays, the designer must discover and solve issues in the early stages of the development cycle. The design consideration should include the intentional and unintentional use of the product. Failure of the headband is not only costly regarding development time, but can also damage the company's quality reputation.

To model the headband component structure a block-diagram was created Figure 1.4. This diagram shows the logical relationships for the headband structure. A headband is constructed from a metal band with a soft pad attached below which will butt against the users head during use. The cables for audio or media control signals are routed between the metal band and headband pad.

By applying the general FMEA form as seen in Table 2.1.1, the FMEA table for headband design can be constructed as in Figure 5.1. The failure modes are identified for "not fit to user's head, headband broken or yield, sound energy leak, and cable fall off after headband bending". These are then cataloged by the functions: headband ergonomic fit, headband security, and acoustic performance. The failure modes have major effects including "not comfortable, cannot be used, lost the bass, and looks bad quality". The

different severities correspond to the effects they have on the headband. Table 4.1.1 is used to assign the severity of an effect. There is more than one root cause for some failure modes in the root cause column. This is because many failures occur when multiple inputs occur simultaneously. Assigning the occurrence; this step is just like ranking the Severity of failure mode effects, but the root cause occurs on a scale of 1 – 10 as rated by frequency based on the Table 4.1.2. Just because the root cause might happen frequently, it doesn't mean we don't know it or can't do anything about. For headband fatigue, the bending cycle test can be conducted to detect failure. This is just a simple example of root cause detection, and there are many other types of controls that can prevent root causes. With effective detection and prevention analysis, we can eliminate root causes from generating failure modes. Table 4.1.3 is used to rate the ability of the detection and prevention methods in finding the root cause. The example question to ask is: "How confident are you that the detection method will find a problem and that prevention techniques will avoid headband fatigue". The detection was assigned a value of 3. This means that the controls have a good chance of detecting the existence of a failure. In fact, over 90% of eminent failures were found in the bending cycle test alone. The other 10% could be due to the manufacturing stability of the process. In this rank system a detection rating of "1" means that the chances of detecting a failure are almost certain. Conversely, a rating of "10" means the detection of a failure or mechanism of failure is absolutely uncertain. After ranking each test, multiply the three ratings—Severity x Occurrence x Detection – to create the risk priority number called RPN for the headband failure modes. This number establishes the relative risk of your failure modes and the root causes of each failure. The final step is to take action resulting from the FMEA.

There are two principles of this method which must be followed in order to choose an appropriate corrective action. One is find ways to reduce the severity of any effect to a ranking of 9 or below. Another is to find ways to reduce any RPN to a value below 100. To summarize the steps for FMEA,

1. Review the design or process
2. Brainstorm potential failure modes
3. List the potential effects of each failure mode
4. Assign *severity* ratings to each of the potential effects
5. Identify the root causes of each failure mode
6. Assign *occurrence* ratings to each root cause
7. Identify the methods of detecting or preventing the root causes.
8. Assign *detection* ratings for the detection methods
9. Calculate the Risk Priority Number (RPN)
10. Develop an action plan for any root cause with an RPN greater than 100

Table 4.1.1: Severity scale used in the study

Scale	Criteria for Severity	Rating
Hazardous (without warning)	Safety issue exists. Will cause harm or property damage	10
Hazardous (with warning)	Safety issue exists. Will cause harm or property damage	9
Extremely High	Device does not work at all. A product return is certain	8
Very High	A major function does not work. Customer's experience is an embarrassment to the brand promise. Significant scrap, rework and sorting. Stop Ship/Build Required.	7
High	End user strongly affected. Customer defection likely. High levels of scrap, rework and sorting. Stop Ship/Build likely…	6
Moderate	Product's secondary functions affected so does not deliver as promised. Problems are noticeable to all customers leading to buyers remorse. Stop Ship/Build probable. Unacceptable levels of scrap, rework and sorting.	5
Low	The product functions as promised but does not deliver to the customer's expectations. Problems are noticeable to average customers and all inspectors. Elevated levels of scrap and rework. Production slows and capacity affected.	4
Very Low	Some effects are noticeable to picky customers. Inspectors finding elevated levels of defects requiring rework. Production yield down.	3
Minor	Minor features affected, cannot be discerned by most users. Slightly elevated levels or rework.	2
Very Minor	No effect visible to the end user or to production inspectors.	1

Table 4.1.2: Root cause occurrence used in the study

Scale	Rate	Rating
Root cause happens all the time	≥ 50%	10
Root cause is present almost all of the time	40%	9
Root cause is present most of the time	30%	8
Root cause is present very often	20%	7
Root cause is present often	10%	6
Root cause is present occasionally	5%	5
Root cause is present not very often	3%	4
Root cause is present infrequently	1%	3
Root cause is present very infrequently	<1%	2
Root cause is never present	0%	1

Table 4.1.3: Root cause detection used in the study

Scale	Criteria for Detection	Rate	Rating
Absolute Uncertainty	No known control(s) available to detect failure mode.	≤ 10% detected	10
Very Remote	Controls have a remote chance of detecting the failure	≤ 20% detected	9
Remote	Controls have a remote chance of detecting the failure	≥ 20% detected	8
Very Low	Controls may detect the existence of a failure	≥ 30% detected	7
Low	Controls may detect the existence of a failure	≥ 50% detected	6
Moderate	Controls may detect the existence of a failure	≥ 70% detected	5
Moderately High	Controls have a good chance of detecting the existence of a failure	≥ 80% detected	4
High	Controls have a good chance of detecting the existence of a failure	≥ 90% detected	3
Very High	The process automatically detects the failure.	≥ 95% detected	2
Almost Certain	Controls will almost certainly detect the existence of a failure	≥ 98% detected	1

4.2 Metal band material selection

Stainless steel (SUS) 301 is selected for the metal band material. Grade 301 belongs to the most commonly used family of stainless steels, which have an austenitic structure at room temperature. This group is resistant to atmospheric corrosion and in atmospheric corrosion conditions (in all but severe marine environments) its clean appearance can be retained indefinitely with little maintenance. Moreover, SUS 301 has a bright, attractive surface making it an excellent choice for this decorative structural application. Compared to the cost of SUS 304, SUS 301 is relatively inexpensive. Therefore, SUS 301 is very suitable for headband material. SUS301 is highly ductile and formable, and has a very high toughness. Grade 301 is formulated to allow the generation of high strength levels by temper rolling to partially transform the structure to martensite. A small proportion of martensite is intimately mixed with the austenite matrix, which provides high strength levels and excellent ductility. Grade 301 is available in a series of different tempers, each of which provide increased strength. These tempers are achieved by increasing the amount of cold rolling reduction during processing at the stainless steel mill. The strength added by cold rolling will be retained, provided that the steel is not heated to the annealing temperature, which is in excess of 600^{o}C.

To select the thickness and tensile strength range for the metal band, material availability in the industry should be investigated. Type 301 is generally used in the annealed and cold-rolled conditions. In the work-hardened condition, Type 301 develops higher tensile strength than the other stable austenitic grades. Minimum properties for plate, sheet and strip per A666 follow (Table 4.2.1). For the thickness of the metal band required, 0.7, 0.75, 0.8, and 0.85mm are available in the industry.

Table 4.2.1: Mechanical Properties, A666 Specifications

Condition	Tensile Strength, Min. Ksi	(MPa)	0.2% Yield Strength, Min. Ksi	(MPa)	Elong. In 2" (50mm) %, Min.
Annealed	75	(515)	30	(205)	40
1/4 Hard	125	(862)	75	(517)	25
1/2 Hard	150	(1,034)	110	(758)	18*
3/4 Hard	175	(1,207)	125	(931)	12*
Full Hard	185	(1,276)	140	(965)	9*

4.3 Design of Experiments

The design of experiment (DOE) method was used to investigate the effects of DVs, such as material and geometry parameters of the headband system, on the output responses, like clamping force and fatigue life. A commercially available software program, DOE++, was used to develop the design of experiments used in this study. The Analysis of Variance (ANOVA) technique was used to predict the relative significance of the DVs and to estimate the experimental errors. As shown in Table 4.3.1, two DVs were chosen in this study: stainless steel headband thickness (t) and stainless steel band tensile strength (σ_u).

Table 4.3.1: Ranges of design variables

Design Variable (DV)	Unit	Lower bound	Upper bound
headband thickness	mm	0.75	0.85
Headband tensile strength	MPa	860	1205

Central composite design was used to develop the response surface methodology (RSM) design. A quadratic response surface model (Equation 4.1) was used to predict the output responses or SVs which are directly related to the headband clamping force, headband fatigue life and cost.

$$d = c_o + \sum_{i=1}^{k} c_i x_i + \sum_{i=1}^{k} c_{ii} x_i^{\,2} + \sum_{\substack{i= \\ i<}} \sum_{\substack{j \\ j}}^{k} c_{ij} x_i x_j \qquad (4.1)$$

This model represents the dependent parameter y (SV) as a function of the main effects of factors (x_i), their interaction ($x_i x_j$), and their quadratic components (x_i^2). Equation 4.1 was used to formulate objective functions for the headband performance characteristics. A central composite design with five center points and alpha = 1.414 is used to conduct the

experiment. Table 4.3.2 shows the DV values for the central composite design used in this study.

Table 4.3.2: DV values used in the central composite design

Design Variables	A: Thickness (mm)	B: Tensile Strength (Map)
$-2^{1/2}$	0.729	803
-1	0.75	873
0	0.8	1040
1	0.85	1207
$2^{1/2}$	0.87	1276

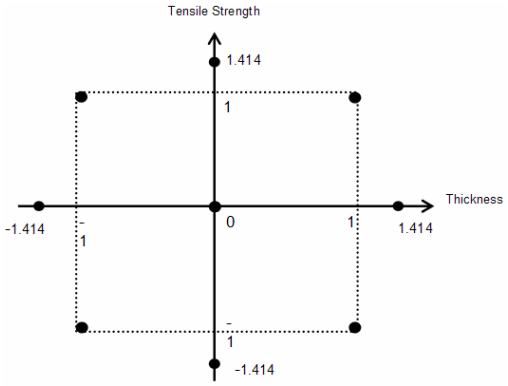

4.4 FEA

Nonlinear finite element method FEM models are widely used to simulate the reliability and performance of structures in industry. Figure 4.4.1 shows the process flow for developing the headband finite element model description.

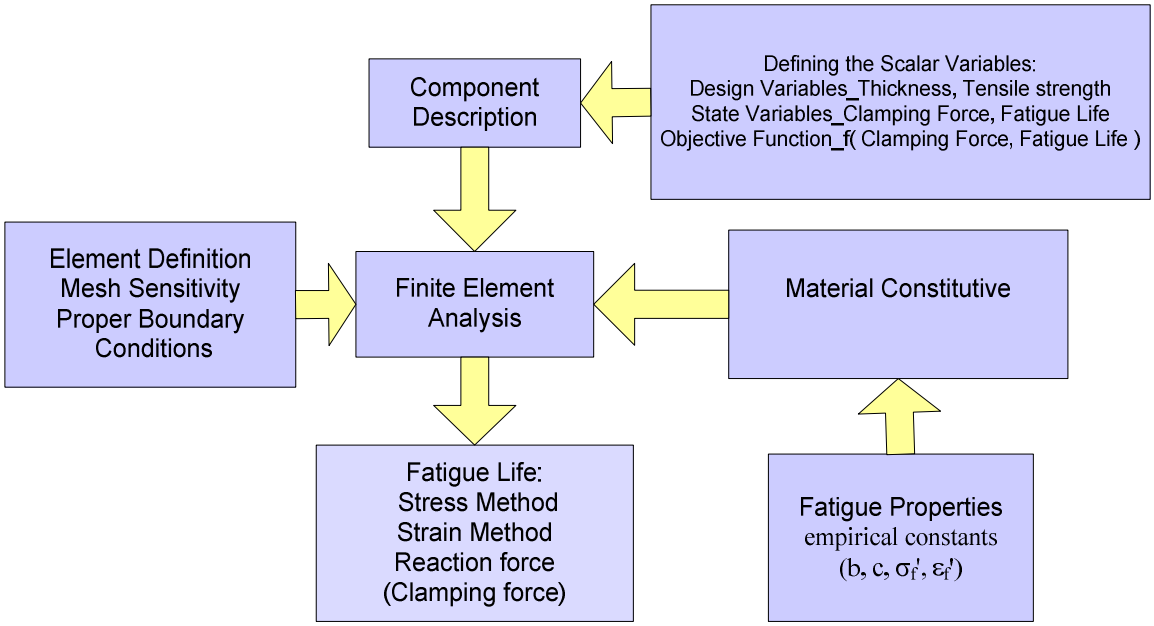

Figure 4.4.1: Flowchart for the finite element modeling

Commercially available FEA software, ANSYS version 11, was used to analyze the maximum shear strain and predict the clamping force and fatigue life of the headband system.

4.4.1 FEM models

The simulation model is constructed as Figure 4.4.2 with varied thickness from 0.87mm to 0.729mm. Considering symmetry, only one half of the entire system has been modeled. The finite element mesh is shown in Fig. 4.4.3.The model is meshed by 42390 three-dimensional eight-node solid elements with 0.3mm element size and 218756 nodes. The different thickness values were each modeled separately Figure 4.4.2 using the same basic FEA model.

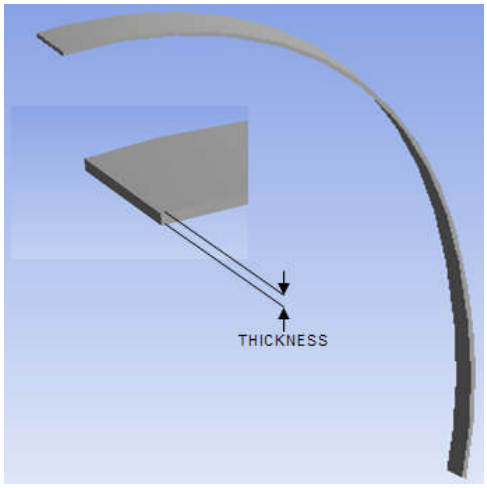

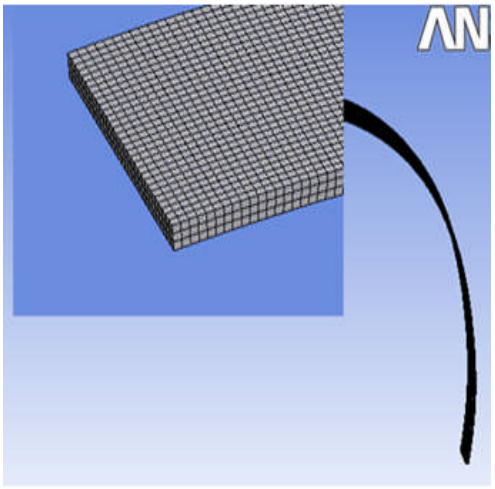

Figure 4.4.2: Model for varied thickness **Figure 4.4.3: Headband mash element**

4.4.2 Boundary conditions

The boundary conditions shown in Figure 4.4.4 represent the real world usage case and correspond directly with the experimental validation. A frictionless support is placed on surface “A” which may move freely in the Y and Z directions, but is constrained in the x direction. An external displacement load applied at the “B” location is pulled along the X direction 75mm. By applying the displacement for a boundary condition; the reaction force will be obtained at thesame location, which will represent the headband clamping force.

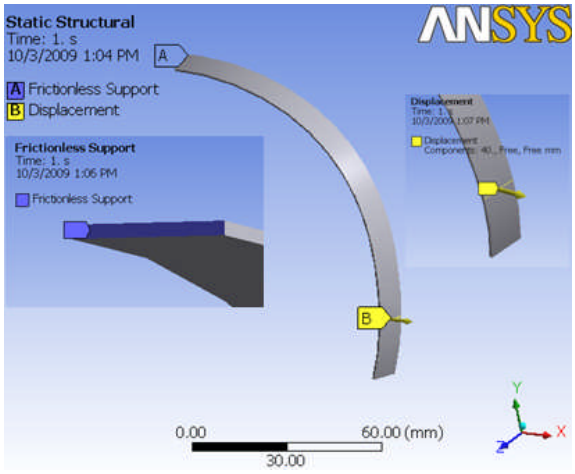

Figure 4.4.4: Headband boundary conditions

4.4.3 FEM material property

In Central Composite Design, headband thickness and varied cold-rolled conditions with varied tensile strengths are the main design variables. The difference in thickness of each headband (Figure 4.4.2) was built into each of the FEA models. A large part of any fatigue analysis is getting an accurate description of the fatigue material properties. The headband is constructed of stainless steel and will be analyzed by SUS 301 with varied cold-rolled conditions (Table 4.2.1). The hardness value of the metal was used to estimate tensile strength. This was then used to estimate the low cycle fatigue properties of metals on the basis of the empirical relations suggested by M.L. Roessle et al. and Julie A. which are described below.

$$\sigma_f' = 4.28HB + 225(MPa) \qquad (2.12)$$

$$\varepsilon_f' = \frac{0.32(HB)^2 - 487(HB) + 191000}{E} \qquad (2.15)$$

b= -0.09

c =-0.6

$n' = b/c$

$K' = \sigma_f'(\varepsilon'_f)^{-n'}$

The material fatigue properties (b, c, σ_f', ε') were calculated according to the equations seen above. Table 4.4.1 shows the material properties for different tensile strength metals used in this study.

Table 4.4.1: Headband material properties used for model

BHN	Ultimate Strength (σ_u) in Mpa	Fatigue Strength Coefficient (σ_f') in Mpa	Fatigue Strength Exponent(b)	Fatigue Ductility Coefficient (ε_f') in MPa	Fatigue Ductility Exponent (c)	Cyclic Strength Coeffici ent (K')	Cyclic Strain Hardening Exponent (n')	Elastic Modulus (E) GPa
235	804	1181	-0.09	0.471	-0.6	1320	0.15	200
255	862	1309	-0.09	0.469	-0.6	1470	0.15	197
297	1034	1487	-0.09	0.432	-0.6	1690	0.15	185
342	1207	1679	-0.09	0.382	-0.6	1940	0.15	178
382	1276	1848	-0.09	0.342	-0.6	2170	0.15	174

By applying displacement for a boundary condition, the reaction force can be obtained at same location, which is representing the headband clamping force. In this study, both stress-life and strain-life theories have been adopted to conduct an accurate and complete fatigue analysis. Considering the mean stress effect, the loading situation of the headband is “zero to maximum”. Here the stress ratio (R) is 0 and amplitude ratio (A) is 1. In direct correspondence with the fatigue properties tested, the ultimate strength approach called the Goodman curve (Figure 2.3.2) is applied. From this the alternative stress is calculated by equation 2.1. By inputting the fatigue properties to ANSYS, the Stress-Life is shown as Figure 4.4.5, and Strain-Life is shown as Figure 4.4.6.. These values were logged for use in later fatigue simulations.

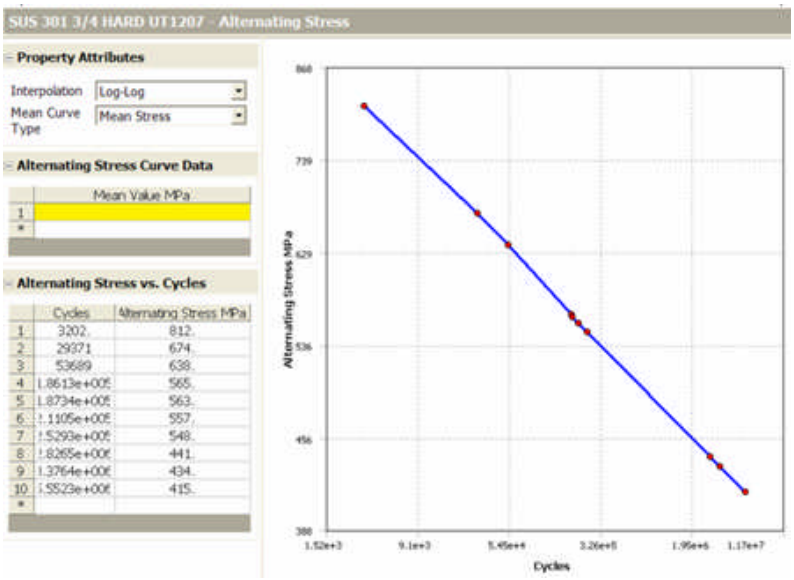

Figure 4.4.5: Stress- Life curve for SUS 301 ¾ cold-rolled

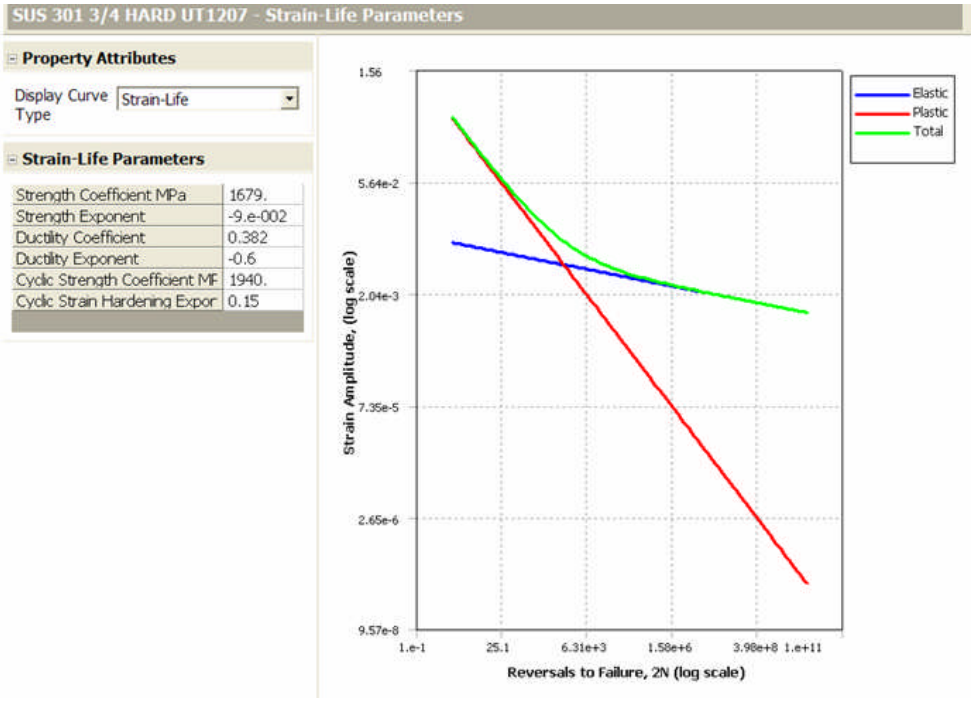

Figure 4.4.6: Strain- Life curve for SUS 301 ¾ cold-rolled

4.5 Experimental verification

4.5.1 Headband strain measurement

To verify the FEA results, a Strain Rosette was set for measuring the principle strains, and max shear strain in the headband**.** To determine the three independent components of plane strain, three linearly independent strain measurements are needed. The strain gage was positioned in a rosette-like layout as in Figure 4.5.1. The gage was then used to measure the strain while the metal headband is experiencing bending motions. Three strain gauges were mounted on the cleaned surfaces of the metal headband with adhesive. The positions for bonding were defined as the center top, ¼ of the length from the bottom, and directly on top of metal band as Figure 4.5.2 shown. Six lead wires were tinned to each strain gauge with their color coded sequentially as demonstrated in Figure 4.5.3. The metal band with strain gauges attached was then installed into the bending machine and connected to the strain gauge meter (Figure 4.5.4). All three strain gauge readings were recorded as metal band was bent to a total 150 mm displacement.

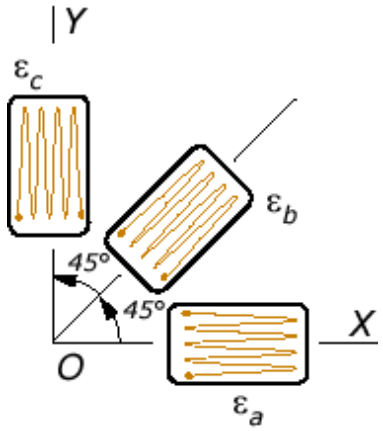

Figure 4.5.1: 45° rosette strain gauge used for measurement [24]

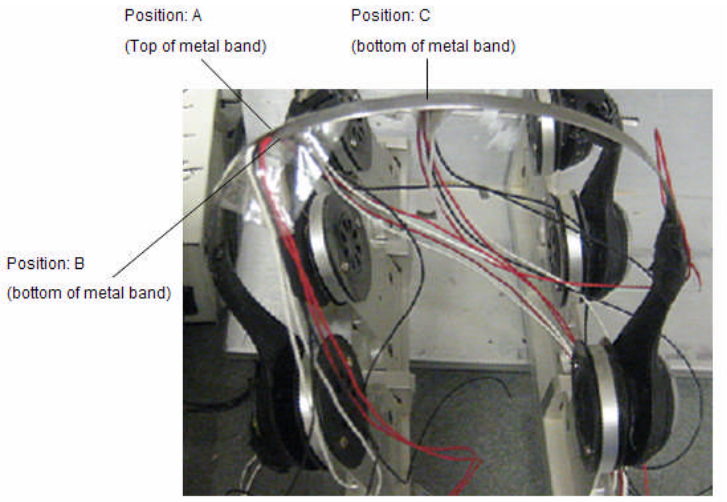

Figure 4.5.2: Strain gauge positions and wiring

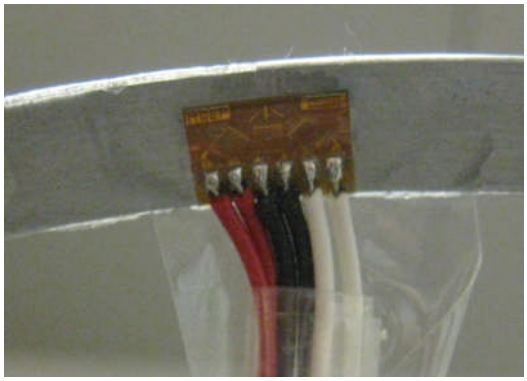

Figure 4.5.3 Strain gauge tinning

Figure 4.5.4: Strain measurement device

4.5.2 Headband force profile measurement of clamping force

To validate the reaction force from FEA results, the force profile was measured in the test machine. One ear cup was clamped by a fixed arm. The other ear cup was clamped by a fixture which has linear movement controlled by a server motor. Both ear cups have ball joint attachment points which provide for freedom of rotation (Figure 4.4.5). The band and ear cup were then cycled 5 times through a 150mm total displacement. The reaction forces were recorded and compared to the displacement of the ear cup in the data acquisition software, Lab View. Figure 5.4 shows the trend lines for the 5 cycles of headband reaction force versus displacement. The reaction force was taking for the data at 150mm displacement from the force profile. This data will then be compared to the FEA results.

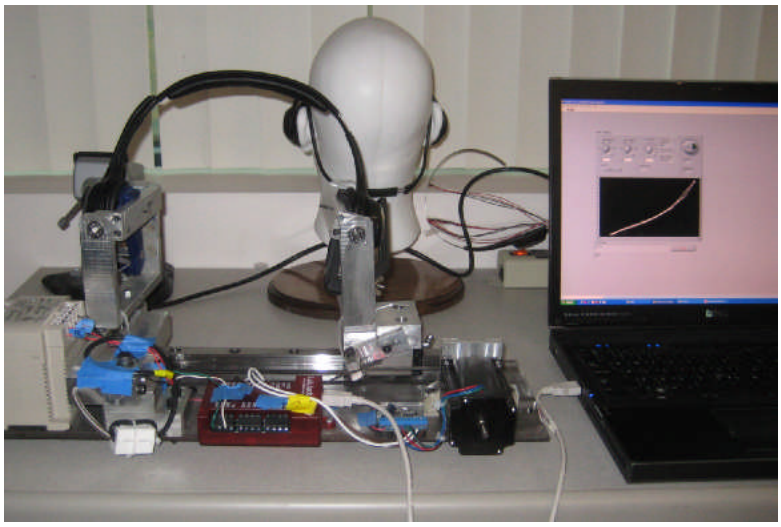

Figure: 4.5.5 Force profile measurement

4.5.3 Bending cycle test for fatigue life

For the bending cycle test, 3 headbands were placed into a bending cycle test machine. Figure 4.5.6 demonstrates how the ear cups were clamped into the fixtures. Similar to the

force profile machine, one side of fixture is fixed, while the other can be moved linearly. The ear cup was moved in the x direction 150mm per cycle. Each complete cycle lasts 5 seconds and this continues until the headband fails. The headband was checked every 500 cycles until complete failure occurred. The total bending cycle was read from the counter on the machine. Due to the slow cycle time, the thermal stress was ignored.

Figure: 4.5.6 Bending cycle test

4.6 Optimization method

This test method utilizes differing hardness values of stainless steel 301. Annealed and cold-rolled steel will be demonstrated to provide different conflicting performance criteria. Thus, there is a need to evaluate solution alternatives according to multiple criteria. Since multiple objective problems rarely have points that simultaneously maximize all of the objectives, it is important to maximize each objective to the greatest extent possible. The first step in this optimization scheme is the formulation of an objective function. It will then be possible to solve the mathematical programming problem. A multiple objective linear program is written as:

$$\text{“max”}\ \{\boldsymbol{C}\,\boldsymbol{x} = \boldsymbol{z} \mid \boldsymbol{x} \in S\} \qquad (4.2)$$

where $\boldsymbol{C}$ is the matrix of objective function coefficients, $\boldsymbol{x}$ is process parameter vector, $\boldsymbol{z}$ is the objective function vector, and S is the feasible region.

The effects of these headband performance parameters will be included in the formulation of an objective function. Here, major headband performance parameters are clamping force, fatigue life, and cost. Thus, d_f (clamping force), and d_N (fatigue life) are chosen for the headband performance parameters in an objective function. For the overall optimization of this design, the headband cost is the most important design criteria. Thus, d_C (Cost) should be added into the objective function. Finally, the multi objective function consists of the sum of each objective using different weight coefficients for each criterion [Enemuoh E., et al 2001]:

$$U(t.\sigma) = \sum_{k=1}^{n} w_k u_k \qquad (4.3)$$

where, $u_k(t,\sigma_u) = \left| \frac{d_k - d_{k_{desired}}}{d_{k_{\max imum}} - d_{k_{desired}}} \right|$ (4.4)

$w_f + w_N + w_C = 1$ (4.5)

$0 \le w_i \le 1$, $i = w_f, w_N,$ *and* w_C

The weighting coefficients w_k are considered to be contribution coefficients of the *k*th headband performance variable to the value of the operation. The choice of weighted coefficients can be accomplished analytically through a trial and error method. However, they are usually determined in part by analytical and graphical means and also by the design engineer based on the relative importance attached to individual performance characteristic. $u_k(t, \sigma_u)$ is the objective function for headband performance in this analysis. D_k is the dependent parameter as a function of the main effects of thickness and tensile strength for the *k*th headband performance as shown in Equation (4.1). Each objective function, $u_k(t, \sigma_u)$ is normalized through the use of constraints on these quality characteristics measures. $D_{kdesired}$ is the desired value for the headband performance. For example, the desired value for the headband clamping force is the 7.5N. The desired value of cost could be zero; however, the headband always has a cost. Thus, a minimum value of cost was chosen as the desired value for the objective function of cost ($d_{Cdesired}$). Finally, each objective function becomes zero when the headband performance parameter is close to the desired value. On the other hand, each objective function approaches one when the headband performance parameter is close to the maximum value.

The multiple objective optimization function can now be formulated as follows:

minimize $U(t, \sigma_u)$

with respect to t and σ_u ,

subject to $t_{min} \leq t \leq t_{maz}$,

$$\sigma_{u\ min} \leq \sigma_u \leq \sigma_{u\ max}$$

$$D_{fmin} \leq D_f \leq D_{fmax},$$

$$D_{Nmin} \leq D_N \leq D_{Nmax},$$

$$D_{Cmin} \leq D_C \leq D_{Cmax},$$

Finally, Figure 4.6.1 presents the concept of optimizing technique on headband design.

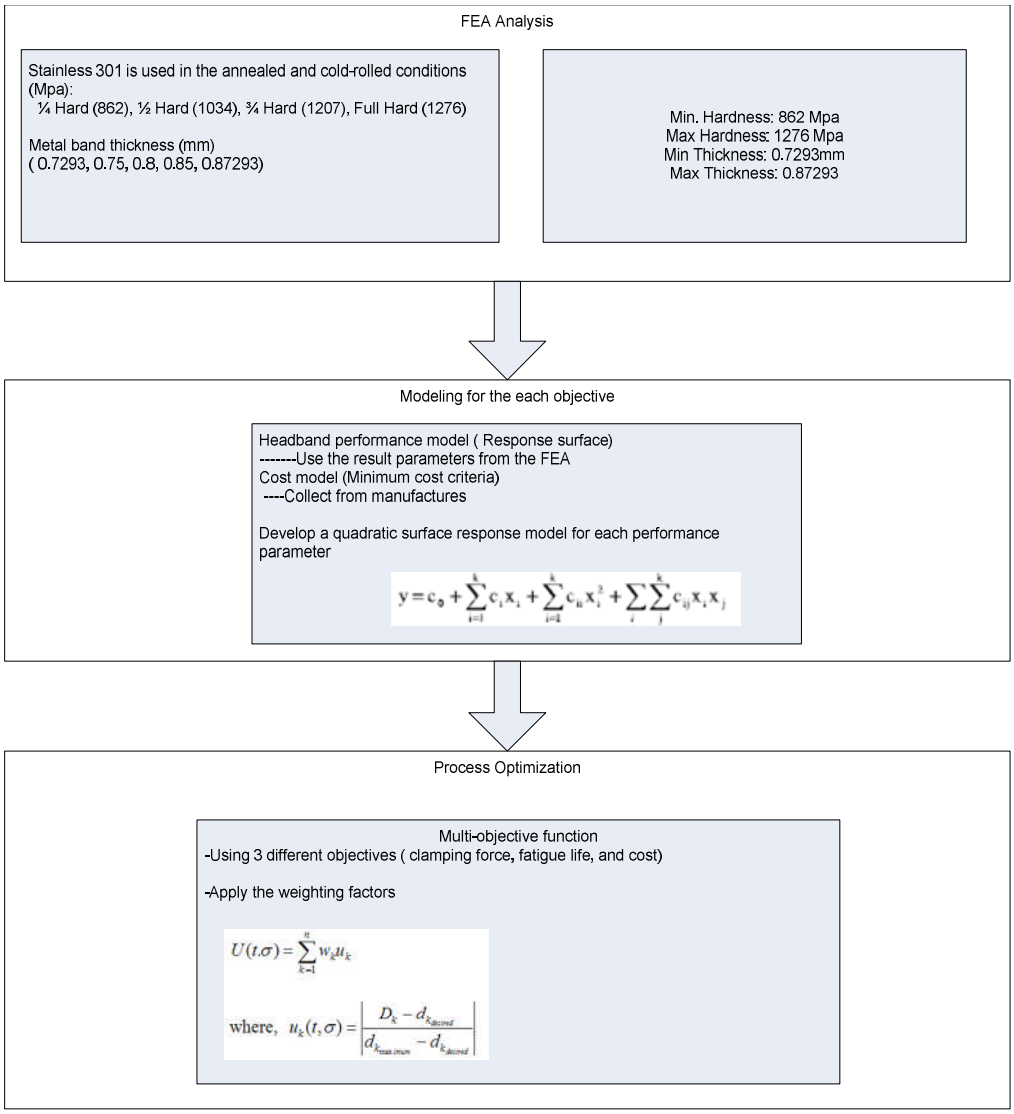

Figure 4.6.1: Basic concept of process optimization for headband design

To optimize the objective function, Eq. (4.1), it is necessary to determine constraints and weight factors. Based on subjective test data, the desired clamping force was selected to be 7.5 N. The minimum fatigue life was estimated to be 25000 cycles and the cost of headband should be held to a minimum.

Determining the appropriate weighting factors is another key in the design optimization using multi-objective functions. In general, the designs engineer can choose the weighting factors based on the relative importance of each objective. The objectives: clamping force, fatigue life and cost had been assigned to be 0.2, 0.4, and 0.4 respectively. DOE software, ReliaSoft's DOE++ is employed to facilitate the principle described above. This software can analyze the data collected from FEA and material providers in order to identify the significant factors and evaluate ways to improve and optimize the overall design. The results of this testing are shown in the Chapter 5.

CHAPTER 5

RESULTS AND DISCUSSION

5.1 Failure Mode Effect Analysis (FMEA) results

FMEA has been successfully conducted on the headband system. The major headband components and their functions were introduced in Figure 1.4. There are three major components in the system: metal band, cabling, and a headband pad. Failure modes and their effect, cause, and detection were identified and are represented in Table 5.1

According to Table 5.1, one failure mode can generate varied effects, each of which can have different root causes. For example, a failure mode, 'Not fit to user's head', creates the effects for 'Not comfortable', 'Not comfortable for long term wear', and 'Loss acoustic bass'. Moreover, the effect, 'Not comfortable' is caused by multiple root causes, such as 'Improper Headband profile for mass population', 'Improper clamping force' and 'Improper manufacture quality for headband profile'.

As shown in Table 5.1, the failure modes with the two highest risk priorities are "Headband fatigue" with RPN of 192 and "Improper headband clamping force" with RPN of 180. Countermeasures are therefore required to reduce the risk of component dissatisfaction or return. Since 'Headband fatigue' and 'Improper headband clamping force' result in the highest risks, urgent actions are required to redesign the headband to reduce the RPN of these items. In order to reduce the RPN of the headband, headband clamping force analysis and headband fatigue analysis have been conducted and presented in the following sections.

Table 5.1: FMEA form for headband design

Project:	xxxxx	Prepared by:	Jason Lin
System / Component:	headband system	FMEA Date (Orig.)	1
Design Responsibility:		FMEA Number:	FMEA-xxx-001
Core Team:		Page:	1 of 1

No	Function/ Process Step	Failure mode	Effect	Sev	Root cause	Occ	Control	Det	RPN		Action
1	Headband ergonomic fit	Not fit to users' head	Not comfortable	5	improper Headband profile for mass population	6	subjective survey	5	**150**		Adjust the headband profile
2	Headband ergonomic fit	Headband is too tight or too loose	Not comfortable	5	Improper clamping force	6	Clamping force measurement & Subjective test	5	**150**		Design review
3	Headband security	headband broken or yield	Can not be used	8	Headband fatigue	8	Bending cycle test	3	**192**		Design Review
4	Headband ergonomic fit	Not fit to users' head	Not comfortable	5	improper manufacture quality for headband profile	7	Go-or-No go gauge, FAI	2	70		Design Review, Work assembly instruction
5	Headband ergonomic fit	Not fit to users' head	Not comfortable	5	improper storage and handling	5	Go-or-No go gauge, FAI	2	50		Work assembly instruction
6	Headband ergonomic fit	Not fit to users' head	Not comfortable for long term wear	4	Improper Headband clamping force due to wrong headband geometry	9	Subjective test, clamping force test	5	**180**		Change the distance between 2 driver cups or headband cross-section change
7	Headband ergonomic fit	Not fit to users' head	Not comfortable for long term wear	4	Improper Headband clamping force due to improper headband material flex module	9	Subjective test, clamping force test	4	**144**		Material change
8	Acoustic performance	Sound energy leak	Loss the bass	4	Not enough headband clamping	9	Subjective test, clamping force test	3	**108**		Change the distance between 2 driver cups or headband cross-section change
9	Headband Cosmetic	Cable fall off after headband bending	Looks bad quality	6	Cable is not secured in the cable channel of headband	4	Bending cycle test	2	48		Add secure feature (under cut hooks)

The risks associated with ‘Headband fatigue’ and ‘Improper headband clamping force’ can be reduced by reducing the severity, reducing the probability of occurrence, or increasing the probability of detection. For example, increasing the metal tensile strength and the thickness of the metal band can immediately improve the fatigue life. This would greatly reduce the probability of occurrence for headband fatigue. However, new failure modes are often created while solving current design or product failures. Using a thicker metal band with high tensile strength may improve the fatigue life of the band, but could seriously impact the cost. Over budget could now be a failure mode for this redesigned system. Therefore the cost should be added to the design parameters, along with the material and geometry of the headband for solving the headband fatigue issue. Incorporating the cost into the design process through the multi-objective function will be presented in Section 5.4.

5.2 Clamping force analysis

5.2.1 Clamping force and Maximum shear strain from FEA

There are 10 sets of design variables which were simulated with ANSYS. For instance, a headband with 0.8mm thickness and ¾ hard cold-rolled stainless 301 (1207 MPa Tensile Strength) was analyzed. A displacement of 75mm along the x-direction with boundary conditions as in Figure 5.1 was employed for this test. A frictionless support at the surface" A" which can move freely in the Y and Z directions, but is constrained in x was also used. The maximum equivalent (von-Mises) stress is obtained to be 627 MPa which is located at the frictionless support outside top corner (Figure 5.2). The Maximum Equivalent Stress is smaller than maximum tensile strength, 1207 MPa, and higher than fatigue strength, 422MPa. The fatigue strength of the material was calculated, based on the Rune Johansson's study, for temper rolled strips of 301 at R (stress ratio) =0. Se/ S_u =0.35 [13]. The reaction force, 8.15N was also calculated from ANSYS simulation and is located where the 75 mm displacement load is applied. This reaction force indicates the headband clamping force. Table 5.2 shows the clamping force simulated by FEM for each set of data analyzed.

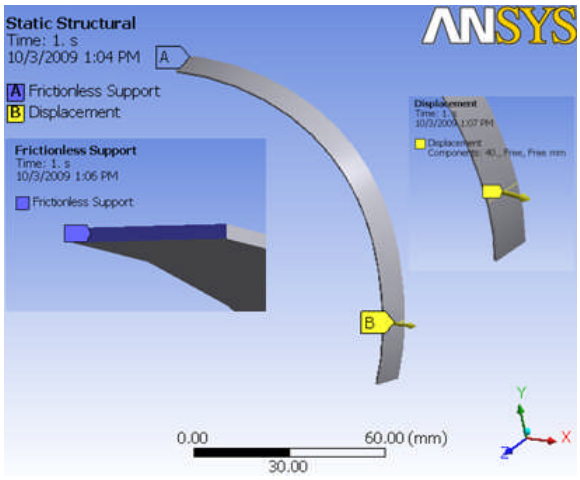

Figure 5.1: Headband boundary conditions

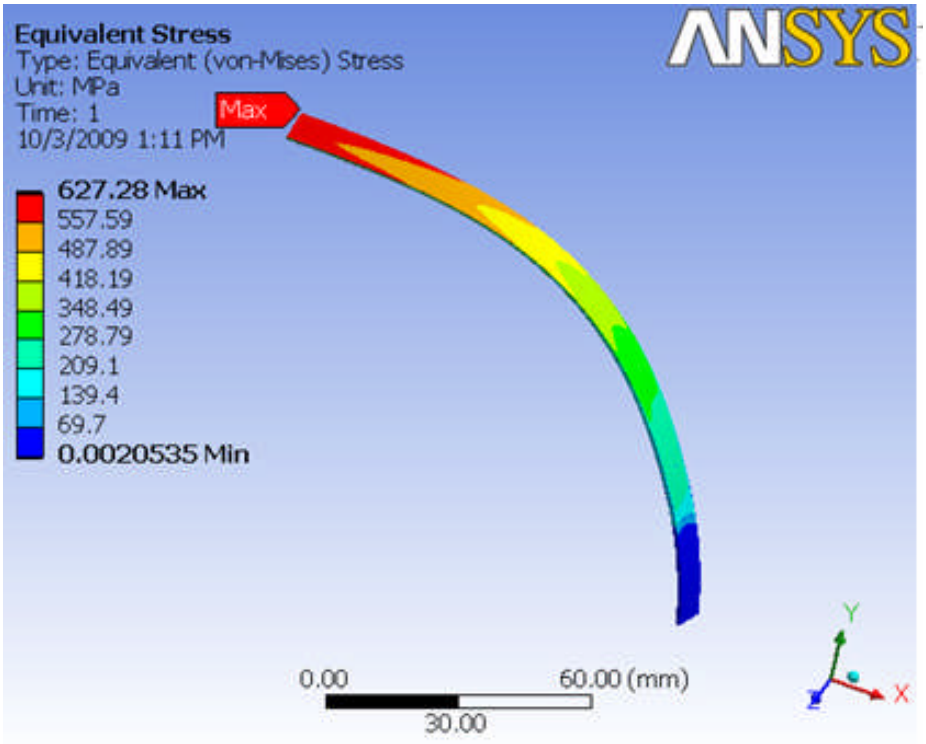

Figure 5.2: Headband von-Mises Stress distribution

Table 5.2: Clamping force for each set

Set	Thickness (mm)	Tensile strength (Mpa)	Clamping force (N)
1	0.7293	1040	6.42
2	0.8	1040	8.47
3	0.87293	1040	10.913
4	0.8	804	9.14
5	0.8	1276	7.96
6	0.75	873	7.28
7	0.75	1207	6.71
8	0.85	873	10.59
9	0.85	1207	9.77
10	0.8	1207	8.15

For validation purposes, the average shear strain values at area “A”, “B” and “C” were obtained when the half band was opened 75 mm from the relaxed state. Figure 5.3a and Figure 5.3b show the average shear strain, 0.004130 mm/mm at chopped corner (position

"C"), 0.002637 mm/mm for position "A" and 0.002743 mm/mm for position "B". These strain values will be compared with the experimental data in the following section.

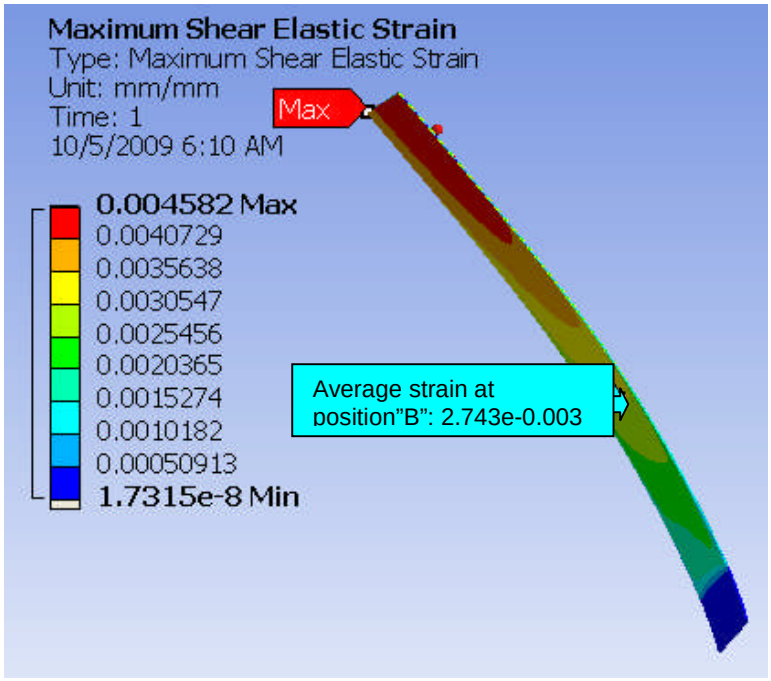

Figure 5.3a: Maximum shear strain- metal band bottom

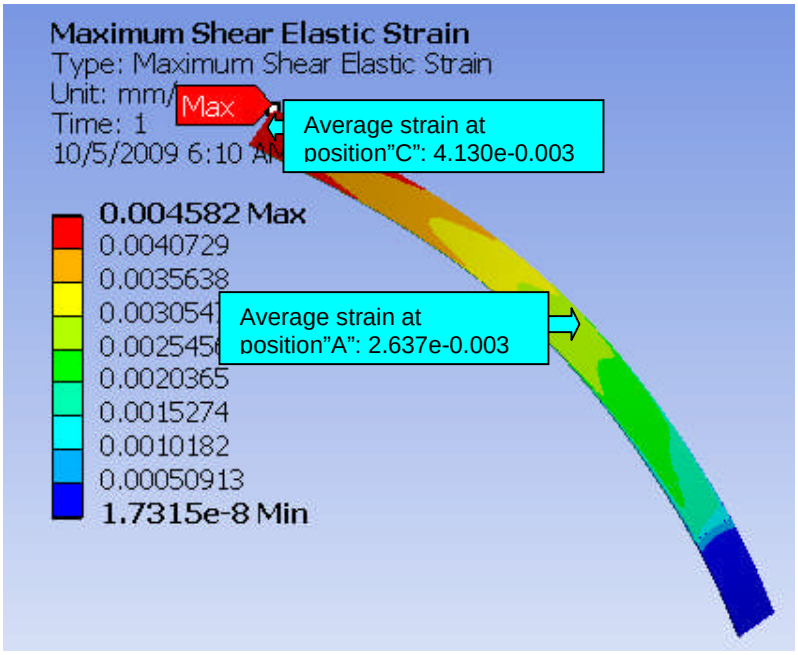

Figure 5.3b: Maximum shear strain- metal band Top

5.2.2 Experimental verification

The shear strains were measured at three positions by the rosette strain gauges. The strain values were obtained when the headband was spread 150mm from its relaxed state. The results were recorded in Table 5.3

Table 5.3: Rosette strain gauge measurement results

Position	Measurement #	ε_a, strain rosette at x-dir (μ)	ε_b, strain rosette at 45 degree (μ)	ε_c, strain rosette at x-dir (μ)
A: 1/4 of total length Top	1	5148	5000	5020
	2	3237	5910	4150
	$\varepsilon_2 - \varepsilon_1$	-1911	910	-870
B: 1/4 of total length bottom	3	5010	5000	5002
	4	3505	6680	5367
	$\varepsilon_4 - \varepsilon_3$	-1505	1680	365
C: Top bottom	5	4992	5002	5001
	6	8352	3178	3845
	$\varepsilon_6 - \varepsilon_5$	3360	-1824	-1156

The principle ε_1, ε_2, and shear strain ε_{xy} were calculated and are shown in Table 5.4. These values are used to compare the shear strain values between the strain gage experiments and the FEA results. The discrepancies are 10.5%, 11% and 10.4% for positions A, B, C respectively see Figure 4.5.2. These discrepancies are probably due to positional errors between the strain gauges, FEA simulation, and force application errors during the strain gauge measurement. However, the three strains all have a consistent error close to 10%; therefore, the FEA results are confirmed by the experiments to a fair degree.

Table 5.4: Principle strains angle from measurement and FEA for three locations

Position	ε_x, Normal strain at x-dir. (μ)	ε_y, Normal strain at y-dir (μ)	ε_{xy}, Normal strain at xy-dir (μ)	θ_p, principle angle (degree)	ε_1, Principle strain at x-dir (μ)	ε_2, Principle strain at y-dir (μ)	ε_{xy}, shear strain (μ)	FEA result for ε_{xy}, Average shear strain (μ)
A: 1/4 of total length top	-1911	-870	2300.5	51.4	968	-3750	2360	2637
B: 1/4 of total length bottom	-1505	365	2250	56.3	1150	-1690	2440	2743
C: center top	3360	-1156	-2926	-26.2	4800	-2590	3700	4130

A headband with a thickness of 0.8mm and made of 3/4 hard cold-rolled (1207 MPa Tensile Strength) 301 stainless steel was tested next. The clamping force and fatigue bending cycle were analyzed by a headband force profile machine and bending cycle test machine respectively.

Figure 5.4 shows the headband force profile. The curve is a trend line averaged by the data from five bending cycle tests. The sixth degree polynomial equation is represented along with the trend curve. At an ear cup distance of 240mm, the clamping force was measured to be 8.1N. This matches the applied 75mm displacement load in FEA where the result of test ten in Table 5.1 (8.15N) almost exactly correlates to the real world findings.

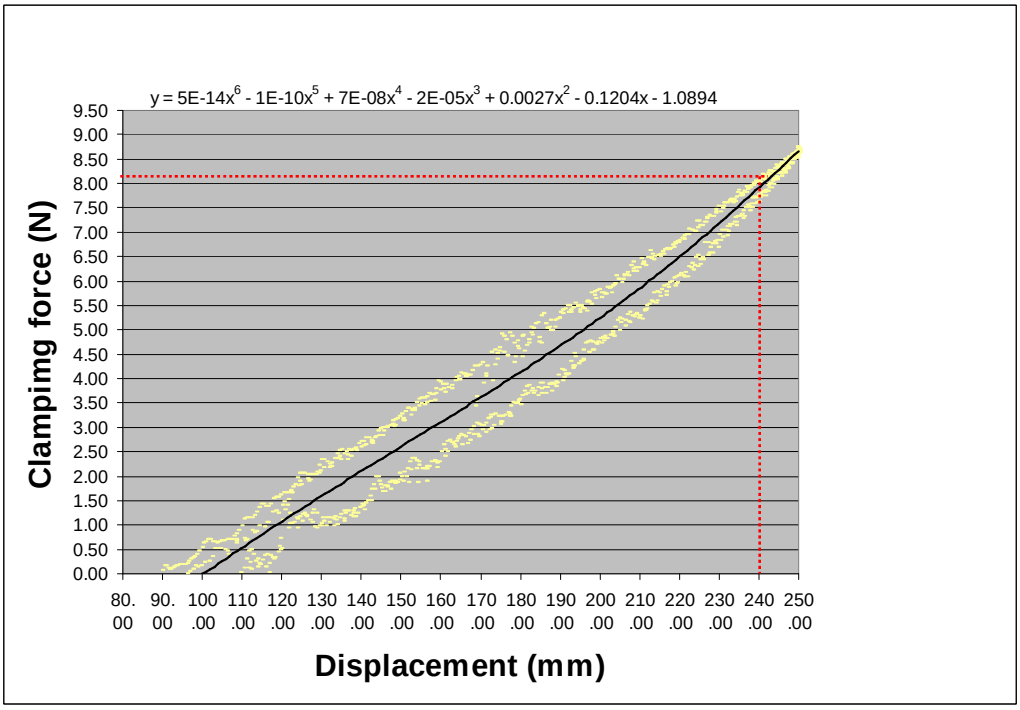

Figure 5.4: Force profile for 0.8mm thickness headband with ¾ hard cold rolled

5.3 Fatigue life analysis

5.3.1 Fatigue life simulation by FEA

For the fatigue life analysis, a 75mm displacement load with the boundary conditions shown in Figure 5.1 was applied to the headband with 0.8mm thickness. This headband is constructed with a ¾ hard cold-rolled stainless steel (Tensile Strength of 1207 MPa). Strain- Life analysis was simulated in ANSYS and the results are shown in Figure 5.5. The headband's minimum fatigue cycle requirement has been determined to be 25,000 cycles. This means that the headband can handle 20 bends every day for 3 years of product life. The estimated headband fatigue strain life is 51,073 cycles, which is 100% longer than the fatigue life requirement (25,000 cycles). In order to verify usefulness of the strain-life method over the stress-life method for the headband analysis, the stress-life analysis has also been conducted in ANSYS. Figure 5.6 shows the results of this analysis and the maximum stress life was found to be 63,849 cycles. The fatigue life from the strain-life method has lower cycles than stress-life due to the plastic region consideration. Julie A. Bannantine [14] stated that strain-life works well for low-cycle applications, and stress-life is suitable for higher cycle applications. The dividing line between low and high cycle fatigue depends on the material being considered, but usually falls between 10 and 10^5 cycles. Therefore, strain life is more appropriate for this headband fatigue life prediction.

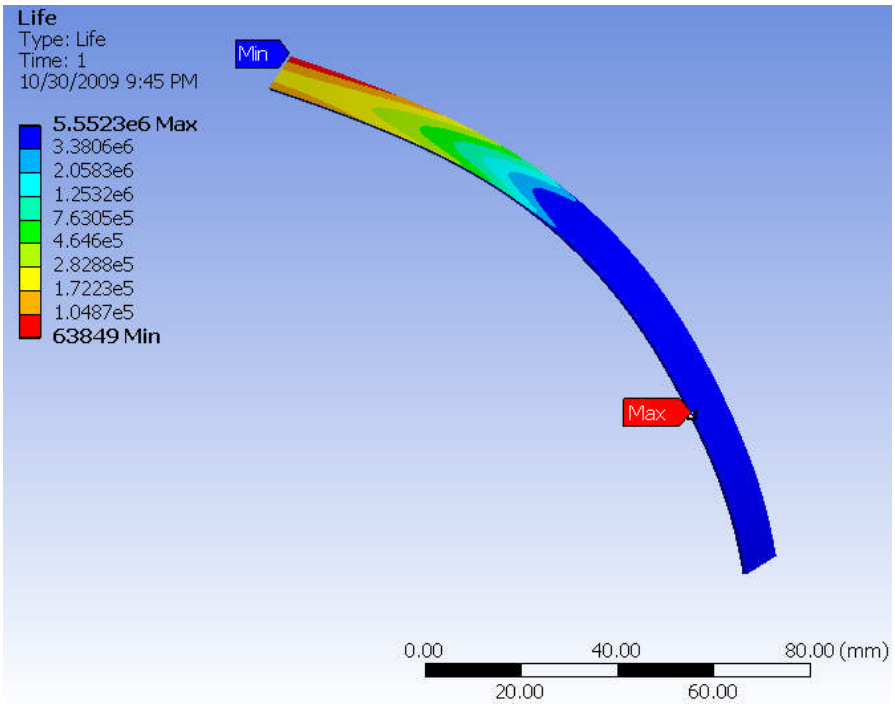

Figure 5.5: Stress-Life for 0.8mm thickness headband with ¾ hard cold rolled

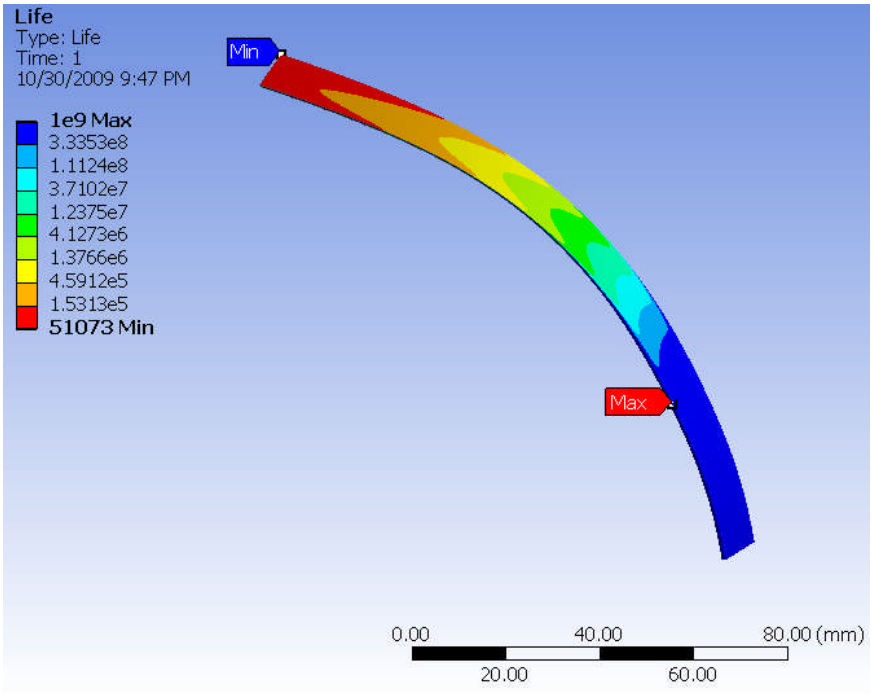

Figure 5.6: Strain-Life for 0.8mm thickness headband with ¾ hard cold rolled

Table 5.5 shows the headband fatigue life for 10 sets of the design factors simulated from ANSYS.

Table 5.5: FEA result for fatigue life

Set	Thickness (mm)	Tensile strength (Mpa)	Von-Mises stress (Mpa)	Estimated Fatigue Life (cycles)
1	0.7293	1040	594.15	13,358
2	0.8	1040	651.95	4,761
3	0.87293	1040	710.23	1,838
4	0.8	804	704.81	155
5	0.8	1276	10	105,290
6	0.75	873	637.45	1,483
7	0.75	1207	587.91	57,912
8	0.85	873	723.09	365
9	0.85	1207	666.89	1207
10	0.8	1207	627.28	51073

5.3.2 Fatigue experiments

Three headband samples were used to conduct the bending cycle tests under the specified loading condition (a displacement of 150 mm). They failed at 76,500 cycles, 88,000cycles and 78,500 cycles, respectively. Comparing the average fatigue life of 81,000 cycles with the fatigue life estimation from FEA (51,073 cycles), only 4.2% error was found in the log scale. Figure 5.7 shows that the headband failed at 76500 cycles from a 1.1mm longitudinal crack. The location of the crack is close to the edge of metal band which corresponds to the maximum shear strain position in the FEA (Figure 5.4(b))

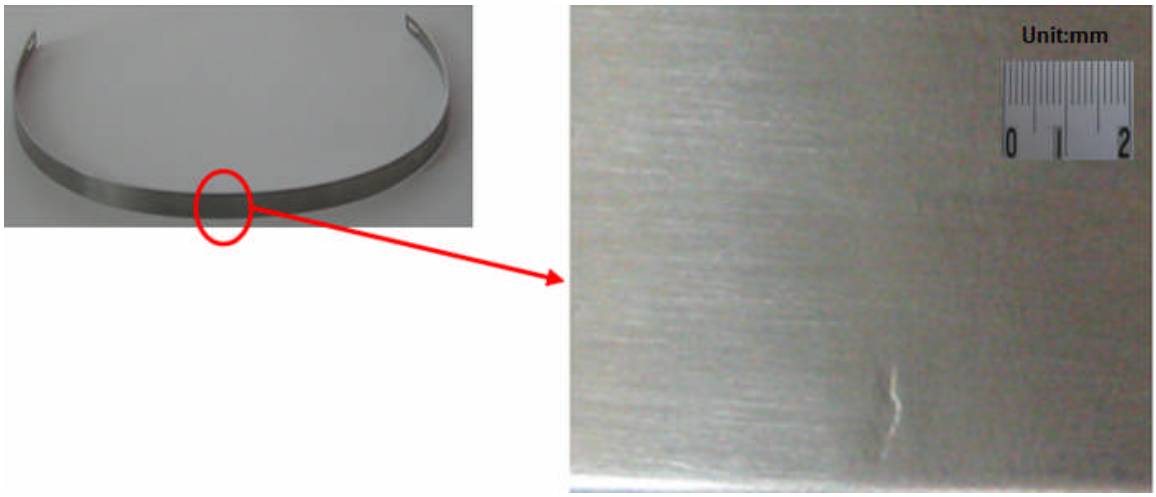

Figure 5.7: Fatigue failed headband sample at 76, 500cycles

In addition, a 15mm permanent deformation of the metal band was found after 76,500 cycles (Figure 5.8). This amount of deflection will greatly impact the headband clamping force. According to Figure 5.4, headband clamping force profile, a 0.7 N clamping force can be expected to reduce the chances that a user will wear the fatigued headband. The crack in the metal band in the figure 5.8 is starting to propagate, and is being plastically deformed by elongation. There is no fracture yet however, but permanent deformation of the metal band is expected. A 15mm permanent deformation also matches the elongation rate (12%) for the SUS 301 with ¾ cold roll found in the table 4.2.1. As the tensile strength is increased by choosing a metal in its cold rolled condition, the ductility of metal band was reduced. Therefore, the metal band has less permanent deformation before rupture for the higher tensile strength of SUS 301, which is another consideration for headband design.

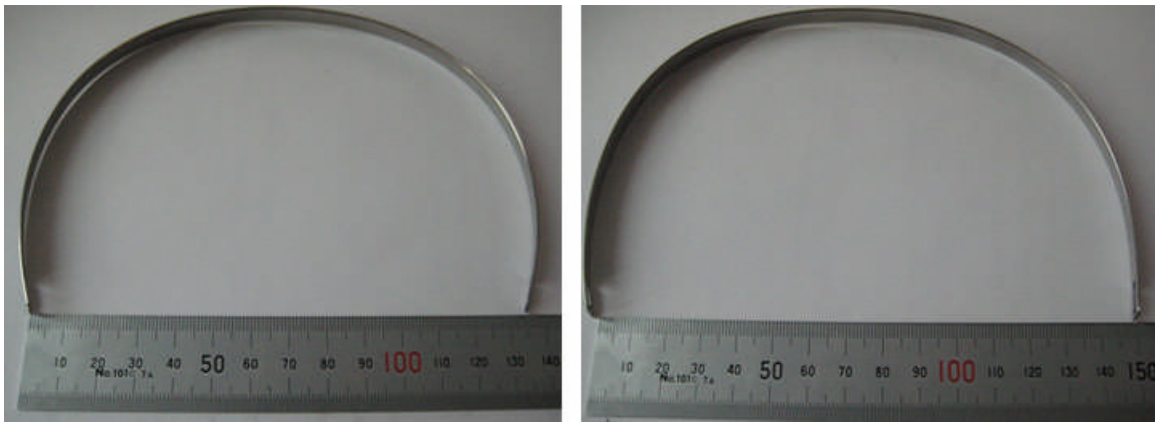

Figure 5.8: Permanent deformation after 76,500 cycles of fatigue test

In conclusion, FEA is a good tool to estimate not only the failure origin location but also the fatigue life.

5.4 Design optimization

Based on the central composite design (CCD) method, the respond data is usually obtained from experiments or calculation. In the headband design, the surface response is constructed by analyzing the metals fatigue life, clamping force and overall cost. Clamping force and fatigue life can be obtained from FEA in the early design stage. The cost data is collected from headband manufactures. The cost data for set #1 and #3 were not given from the manufacturers, because the thickness of 0.873mm and 0.729mm are not available. Therefore, the cost for these sets was estimated through linear interpolation. Table 5.6 summarizes the design variables (thickness and tensile strength) and the responses (fatigue life, clamping force, and cost).

Table 5.6 fatigue life, clamping force and cost data summary

	Design variables		Responses		
Set	Thickness (mm)	Tensile strength (Mpa)	Fatigue Life	Clamping force (N)	Cost (dollar)
1	0.7293	1040	13,358	6.42	0.41
2	0.8	1040	4,761	8.47	0.51
3	0.87293	1040	1,838	10.913	0.73
4	0.8	804	155	9.14	0.49
5	0.8	1276	105,290	7.96	0.55
6	0.75	873	1,483	7.28	0.47
7	0.75	1207	57,912	6.71	0.5
8	0.85	873	365	10.59	0.66
9	0.85	1207	1207	9.77	0.71
10	0.8	1207	51073	8.15	0.53

For the clamping force, the thickness has a greater impact than the material condition selected. As shown in Figure 5.9, the reaction force can be dominated by maximum von-Mises stresses, which is mostly affected by the sample thickness and the modulus of elasticity. Table 4.4.1 shows a slight change for the elastic modulus for the different cold-rolled conditions. Therefore, the thickness is the major factor for the variation of the reaction force.

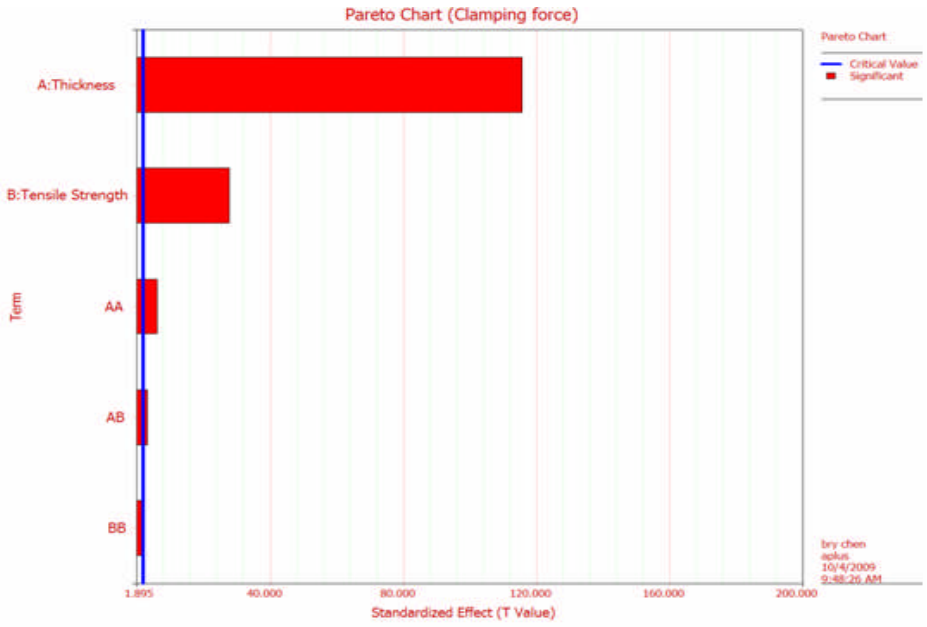

Figure 5.9: Factor effect for clamping force

The equation for the clamping force was obtained through regression analysis. Equation 5.1 represents the clamping force surface model.

f = -0.47327-7.4271 t+ 9.54977 *10^{-4} σ_u+29.21263 t^2+1.32402 *10^{-6} σ_u^2 -7.48503 *10^{-3} t*σ_u (Eq. 5.1)

R^2 = 0.9994

Equation 5.1 was plotted in a 3D space and shown in Figure 5.10. The response surface is helpful when trying to identify relationship trends. This in turn helps to offer physical explanations for the observed relationships under these constraints.

If the desired clamping force of 7.5 N is the only design consideration, then the combination of 0.779mm thickness and 1207Mpa tensile strength will be the optimal design variables. Figure 5.11 indicates the design variables that result in a clamping force of 7.5 N.

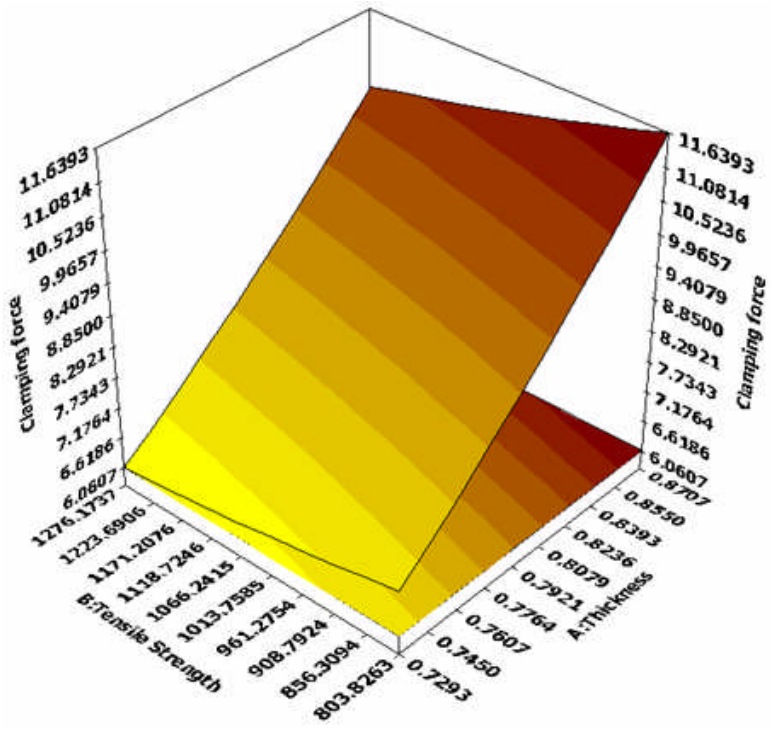

Figure 5.10: Surface plot for clamping force

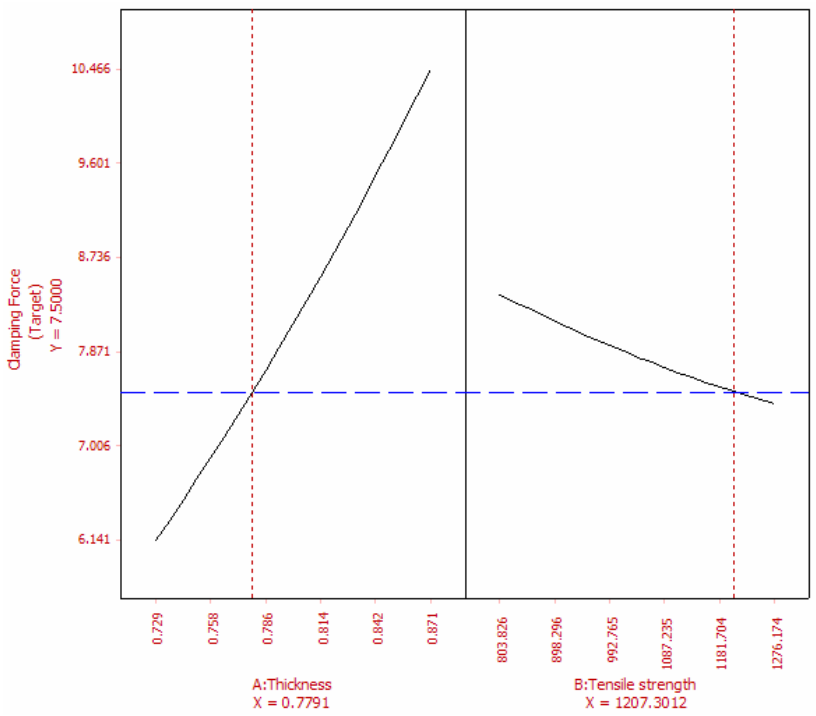

Figure 5.11: Optimal Objective function for clamping force

In order to find the effect of the design variables on fatigue life, an analysis of variance has been conducted. As shown in Figure 5.12, the tensile strength of the metal band plays the most important role in fatigue life analysis. The thickness is not as critical as the strength. The results seem to be reasonable because the fatigue strength coefficient (σ_f') and the cyclic strength coefficient (K') are dramatically increased by adding the tensile strength from the varied cold-rolled conditions. After conducting the response surface modeling analysis, Equation 5.2 can be formulated. Figure 5.13 is the fatigue life surface model described by equation 5.2.

N= -1.04316*10^6+2.65807 *$10^6 t$ -45.65756σ_u-6.92924 *$10^5 t^2$+0.73640σ_u^2-

1664.28144t*σ_u (Eq.5.2)

R^2 = 0.8512

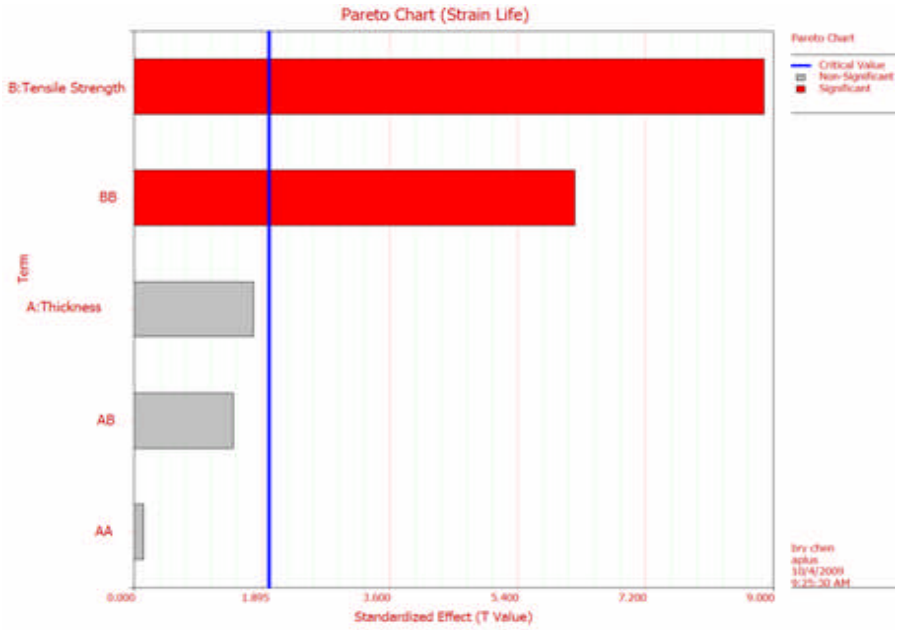

Figure 5.12: Factor effect for strain life

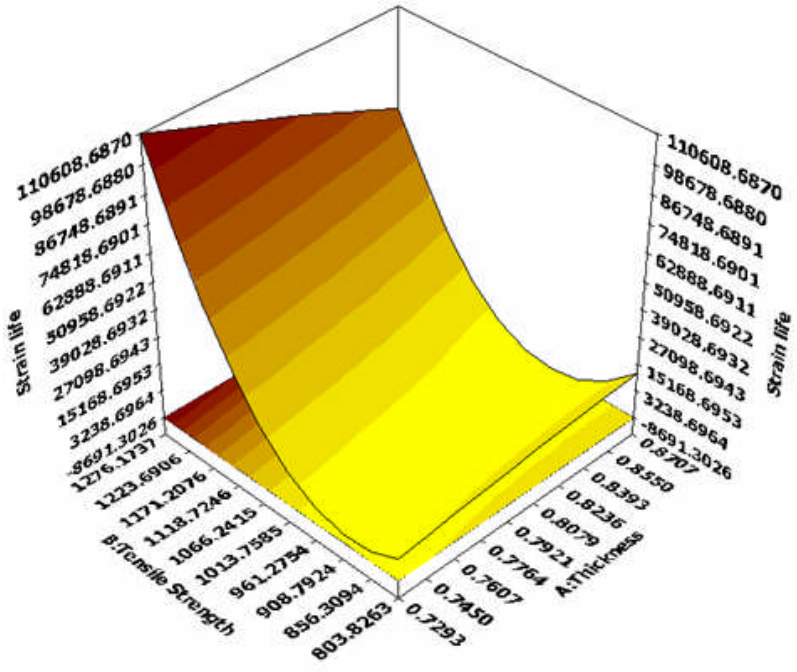

Figure 5.13: Surface plot for strain life

If the required fatigue life of 40,000 cycles is the only design consideration, the optimal solution can be the combination of 0.79mm thickness and 1176 MPa tensile strength (Figure 5.14).

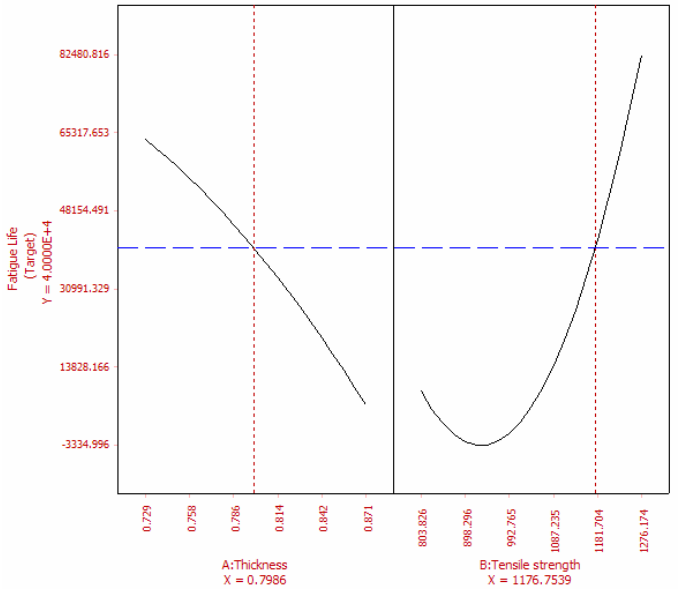

Figure 5.14: Optimal objective function for fatigue life

When it comes to headband cost, the thickness has more impact than the tensile strength as shown in Figure 5.15. However, the tensile strength is still to be considered as a critical variable. Both thickness and tensile strength should be considered for overall optimization of the headband cost.

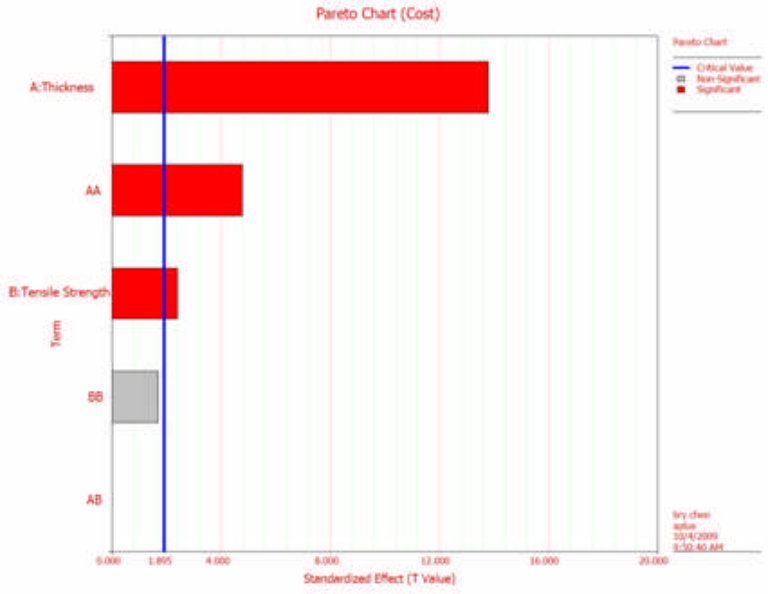

Figure 5.15: Factor effect level for cost

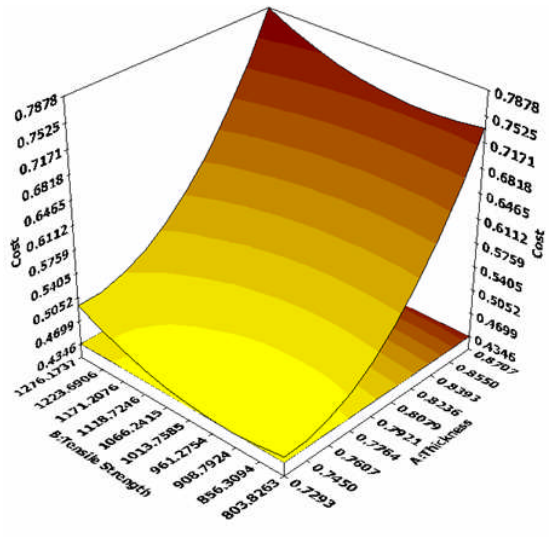

Figure 5.16: Surface model for cost

The cost model corresponds to the surface model in Figure 5.16 and can be described with equation 5.3.

$$C=10.2998-24.6044t-1.635*10^{-3}\,\sigma_u+16.2979\,t^2+6.11360*10^{-7}\,\sigma_u^{\,2}+5.988*10^{-4}\,t*\sigma_u$$

(Eq. 5.3)

$R^2 = 0.9618$

If the minimum cost is the only design consideration, then a thickness of 0.735mm and 961MPa tensile strength will be the optimal solution for the design variables (Figure 5.17)

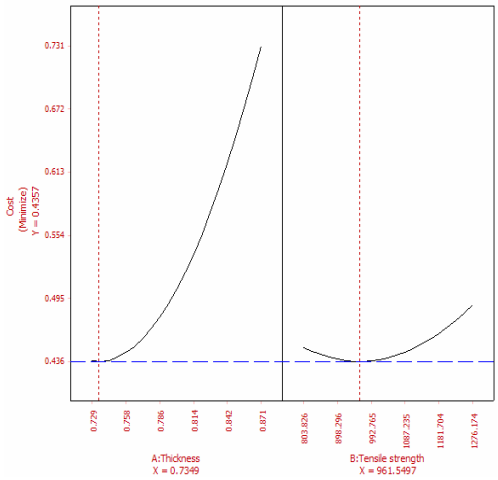

Figure 5.17: Optimal objective function for cost

When designing the headband, there arises the need to evaluate solution alternatives according to multiple criteria. Since multiple objective problems rarely have points that simultaneously maximize all of the objectives, it is important to maximize each objective to the greatest extent possible. The first step in this optimization scheme is the formulation of a decision-maker's objective function. Then a solution of the mathematical programming problem can commence. The effects of the design variables are included in formulating an objective function. The multiple objective linear function is written as:

$U(t, \sigma) = \sum w_i u_i$

Finally, the t multiple objective linear function for headband design is written as:

$$u_k(t,\sigma_u) = \left| \frac{D_k - d_{k_{desired}}}{d_{k_{maximum}} - d_{k_{desired}}} \right|$$

$u_k(t,\sigma_u)$ is the objective function for *k*th response variable. D_k is the dependent parameter as a function of the main effects of thickness and the tensile strength for the *k*th response variable. These are Equations 5.1, 5.2, and 5.3. The weighting factors, w_i, should also be determined. For this study, the weighting factors were determined as 0.2 for the clamping force, 0.4 for the fatigue life, and 0.4 for the cost. The sum of these weighting factors becomes 1.

By setting the desired clamping force of 7.5 N with a weighted factor of 0.2, the fatigue life of 40,000 cycles receives a weight of 0.4, and the minimum cost is weighted 0.4 for the optimal headband design. These optimal design variables are shown in Figure 5.18. The combination of thickness equals 0.7759 mm and tensile strength equals 1154 MPa results in the optimal output response values. These are 7.5 N of clamping force, 40000 cycles of fatigue life and 0.48 dollar for the cost. Based on industry availability, a

headband with 0.8mm of thickness and constructed of ¾hard cold-rolled steel (1207MPa of tensile strength) with cost 0.53 dollar has been selected for the optimal design variables for production.

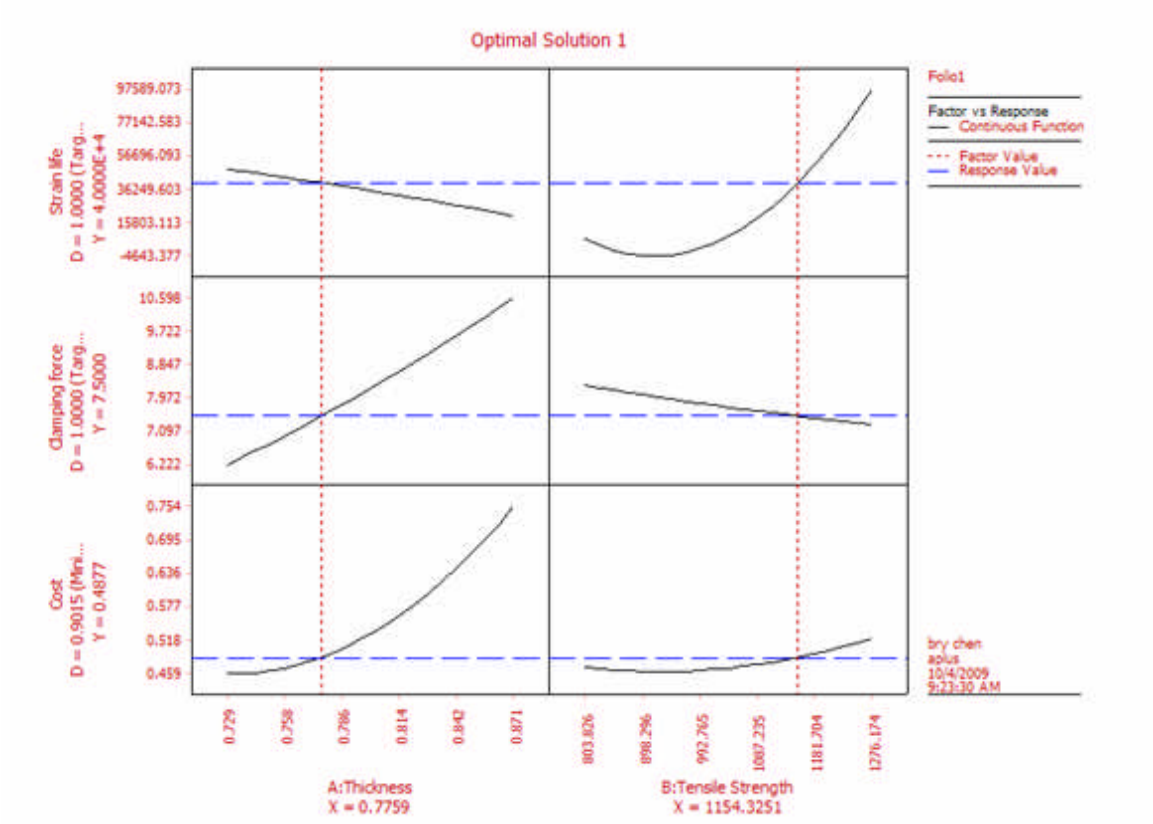

Figure 5.18: Optimal solution for headband design with weight 0.2 for clamping force, 0.4 for fatigue life and 0.4 for cost.

CHAPTER 6

CONCLUSIONS

The FMEA of Headband design is a structured, qualitative analysis of a system for the purpose of identifying potential system failure modes, their causes and the effects associated with each potential failure mode's occurrence. Two high risk failure modes are improper clamping force and headband fatigue failure. Both failure modes are dominated by two design factors, metal band thickness and tensile strength.

Finite Element Analysis (FEA) was used to predicate the design responses, which are headband fatigue life and clamping force. In order to verify the FEA results, strain measurement, reaction force measurement and bending cycle experiments were conducted. There was good agreement between the FEA results and the experimental data.

With the FEA results and cost analysis data, the headband design (metal band thickness and tensile strength) was optimized using the multi-objective function. As a result of this optimization, the 0.8 mm thickness metal band with 1207MPa tensile strength proved to be the optimal design. The design methodology flow is very suitable in the headband development industry, particularly when applied in the early design phase. This analysis ensures that design integrity and optimal performance can be achieved efficiently and at a low cost to the developer and the customer.

A plastic headband and improved headphone comfort are great ideas for future headphone design studies. Plastic can easily replace metal in many circumstanced and is beneficial in light weight and cost efficiency areas. However, plastic has different material behaviors in relation to fatigue life and would need to be thoroughly tested

before implementation. The Smith-Watson-Topper equation for strain-life might need to be revised or extended for this correction. Furthermore, plastic is much more likely to suffer from process defects than metal band structures. For instance, the molding defects and injection gate location could easily alter the fatigue properties of the plastic headband. Therefore, the study should consider the principle polymer properties and employ proper process defect analysis before building a plastic headband. For the comfort study, the optimal headband clamping force, ear pad pressure distribution and ear pad material can be researched by both objective measurement and subjective survey to improve the headphone ergonomics. Moreover, the overall design of the headband can be modified to fit a wider range of head sizes and shapes.

BIBLIOGRAPHY

[1] KIM, Sung-Il. The structure for head-phone. World Intellectual Property Orgnization Website. Available at: http://www.wipo.int/pctdb/en/wo.jsp?IA=KR2002000213. Accessed October 15, 2008.

[2] Seung J. Rhee, Kosuke Ishii. Using cost based FMEA to enhance reliability and serviceability. Advanced Engineering Informatics. 2003; 17: 179–188

[3] Lawrence P. Chao, Kosuke Ishii. Design Process Error Proofing: Failure Modes and Effects Analysis of the Design Process. Journal of Mechanical Design. 2007; 129: 491-501

[4] Stock M, Stone R, Tumer IY. Going back in time to improve design: the function-failure design method. In: Proceedings of the 2003 ASME design engineering technical conference, design theory and methodology conference, DETC2003/DTM-48638, Chicago, USA

[5] Strawbridge Z, McAdams DA, Stone RB. A computational approach to conceptual design. In: Proceedings of the 2002 ASME design engineering technical conference, design theory and methodology

[6] Robert B. Stone Æ Irem Y. Tumer Æ Michael E. Stock. Linking product functionality to historic failures to improve failure analysis in design. Research in Engineering Design, 2005; 16: 96–108

[7] G. Arcidiacono, G. Campatelli. Reliability Improvement of a Diesel Engine Using the FMETA Approach. *Qual. Reliab. Engng. Int.*2004; 20:143-154

[8] Paulo Henrique Trombetta Zannin, Samir N.Y. Gerges. Effects of cup, cushion, headband force, and foam lining on the attenuation of an earmuff. International Journal of Industrial Ergonomics. 2006; 26: 165–170

[9] C Jordan, R Bartlett. Pressure distribution and perceived comfort in casual footwear. Gait & Posture. 1995; 3:215-210

[10] Yeh-Liang Hsu, Chung-Cheng Huang, Chin-Yu Yo, Chiou-Jong Chenb, Chun-Ming Lien. Comfort evaluation of hearing protection. International Journal of Industrial Ergonomics. 2004; 33: 543–551

[11] S. Kwofie , H.D. Chandler. Fatigue life prediction under conditions where cyclic creep–fatigue interaction occurs. International Journal of Fatigue. 2007; 27: 2117–2124

[12] Basquin, O. H. The Exponential Law of Endurance Tests. Proc. ASTM. ;1910: 625-630.

[13] S. Kwofie. An exponential stress function for predicting fatigue strength and life due to mean stresses. International Journal of Fatigue. 2001; 23: 829–836

[14] Rune Johansson and Hans Nordberg. Fatigue properties of stainless steel strip

[15] Julie A. Bannantine, Jess L. comer and James l. Handrock, Fundamentals of Metal Fatigue Analysis. Prentice Hall;1989: 40-64

[16] M.L. Roessle 1, A. Fatemi. Strain-controlled fatigue properties of steels and some simple approximations. International Journal of Fatigue. 2000; 22: 495–511

[17] David J. Jones and Peter Kurath, "Cyclic Fatigue Damage Characteristics Observed for Simple Loadings Extended to Multiaxial Life Prediction", NASA Contractor Report 182126, June. 1988

[18] Yan-Hui Zhang , Stephen J. Maddox. Fatigue life prediction for toe ground welded joints. International Journal of Fatigue. 2009; 31:1124–1136

[19] Lawrence FV, Mattos RJ, Higashida Y, Burk JD. Estimating the fatigue crack initiation life of welds. In: Hoeppner DW, editor. Fatigue testing of weldments, ASTM STP 648. American Society for Testing and Materials; 1978: 134–58.

[20] Lulu, M. Designing Quality and Reliability into Circuits. Qual. Eng., 1996: 383–393.

[21] Lulu, M., and Magsoodloo, S. Analytically Intractable Failure Events. Qual. Eng. 2003; 16(2):283–288.

[22] Strawbridge Z, McAdams DA, Stone RB. A computational approach to conceptual design. In: Proceedings of the 2002 ASME design engineering technical conference, design theory and methodology

[23] Kim, D., and Ramulu, M. Drilling process optimization for graphite/bismaleimide-titanium alloy stacks. Composite Structures. 2004; 63:101-114

[24] Mohammad M. Hossain, Sudhakar G. Jagarkal and Dereje Agonafer. Design Optimization and Reliability of PWB Level Electronic Packag. Journal of Electronic Packaging. 2008; 129: 9-17

[25] Tong Hong Wang, Ching-Chun Wang, Yi-Shao Lai, Kuo-Chin Chang, Chien-Hsun Lee. Optimization of board-level thermomechanical reliability of high performance flip-chip package assembly. Microelectronic Engineering. 2008; 85: 659–664

[26] Willlam F. Riley, Leroy D. Sturges and Don H. Morris., " Mechanics of Materials 5th ed", John Wiley & Sons, Inc., PP. 121, 122, 126 and 131-138, 1999.

[27] Strain Gage Rosettes: Selection, Application and Data Reduction, VISHAY micro – measurements, Tech Note 515

[28] D. Alfred Hancq, “Fatigue Analysis Using ANSYS”, Ansys Inc.

APPENDIX

SUS 301, TENSILE STRENGTH 804MPa

$\sigma_{uts\ (ultimate\ strength\ Mpa)}$	b (fatigue strength exponent)	σ (stress, Mpa)	N (fatigue life, cycles)
1181	-0.09	812	32.11290932
1181	-0.09	674	254.4049586
1181	-0.09	638	468.1723596
1181	-0.09	565	1806.191903
1181	-0.09	563	1878.778539
1181	-0.09	557	2116.302813
1181	-0.09	548	2536.20809
1181	-0.09	441	28341.90146
1181	-0.09	434	33856.22551
1181	-0.09	415	55674.54559
1181	-0.09	530	3675.768006

SUS 301, TENSILE STRENGTH 862MPa

$\sigma_{uts\ (ultimate\ strength\ Mpa)}$	b (fatigue strength exponent)	σ (stress, Mpa)	N (fatigue life, cycles)
1309	-0.09	812	100.7470687
1309	-0.09	674	798.1386422
1309	-0.09	638	1468.786039
1309	-0.09	565	5666.523013
1309	-0.09	563	5894.247345
1309	-0.09	557	6639.426617
1309	-0.09	548	7956.785483
1309	-0.09	441	88916.37519
1309	-0.09	434	106216.3332
1309	-0.09	415	174666.4313
1309	-0.09	530	11531.89978

SUS 301, TENSILE STRENGTH 1034MPa

$\sigma_{uts\ (ultimate\ strength\ Mpa)}$	b (fatigue strength exponent)	σ (stress, Mpa)	N (fatigue life, cycles)
1487	-0.09	812	415.402714
1487	-0.09	674	3290.904266
1487	-0.09	638	6056.13359
1487	-0.09	565	23364.3427
1487	-0.09	563	24303.30109
1487	-0.09	557	27375.84202
1487	-0.09	548	32807.60748
1487	-0.09	441	366622.1167
1487	-0.09	434	437953.7159
1487	-0.09	415	720188.7911
1487	-0.09	530	47548.60392

SUS 301, TENSILE STRENGTH 1207MPa

$\sigma_{uts\ (ultimate\ strength\ Mpa)}$	b (fatigue strength exponent)	σ (stress, Mpa)	N (fatigue life, cycles)
1679	-0.09	812	3202.552802
1679	-0.09	674	25371.27063
1679	-0.09	638	46689.84323
1679	-0.09	565	180127.7138
1679	-0.09	563	187366.6261
1679	-0.09	557	211054.4216
1679	-0.09	548	252930.6904
1679	-0.09	441	2826478.132
1679	-0.09	434	3376410.053
1679	-0.09	415	5552305.155
1679	-0.09	530	366576.6004

SUS 301, TENSILE STRENGTH 1276MPa

$\sigma_{uts\ (ultimate\ strength\ Mpa)}$	b (fatigue strength exponent)	σ (stress, Mpa)	N (fatigue life, cycles)
1848	-0.09	812	4647.915248
1848	-0.09	674	36821.72408
1848	-0.09	638	67761.70378
1848	-0.09	565	261422.1839
1848	-0.09	563	271928.1312
1848	-0.09	557	306306.6014
1848	-0.09	548	367082.2889
1848	-0.09	441	4102112.165
1848	-0.09	434	4900237.012
1848	-0.09	415	8058147.794
1848	-0.09	530	532018.3854

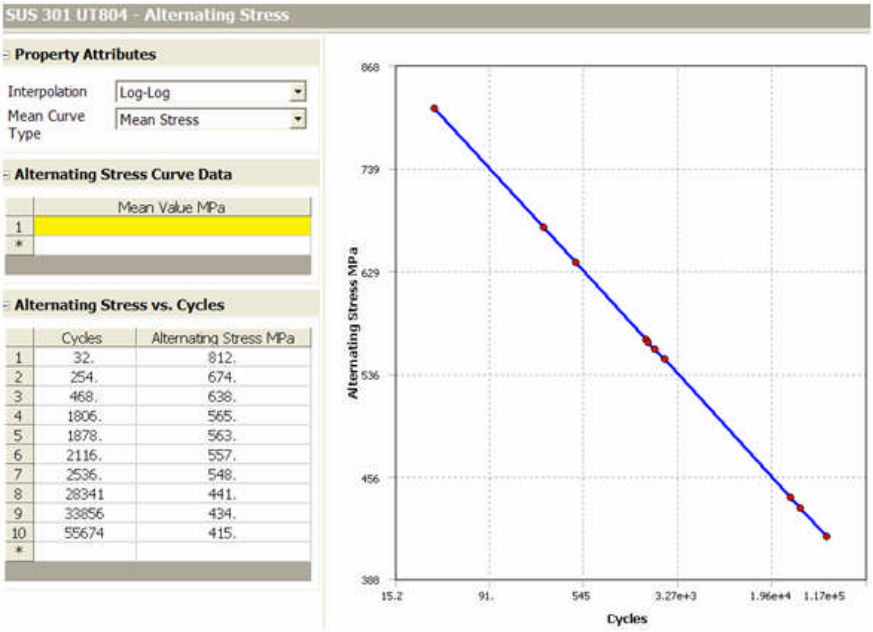

Stress- Life curve for SUS 301 , 804 MPa tensile strength

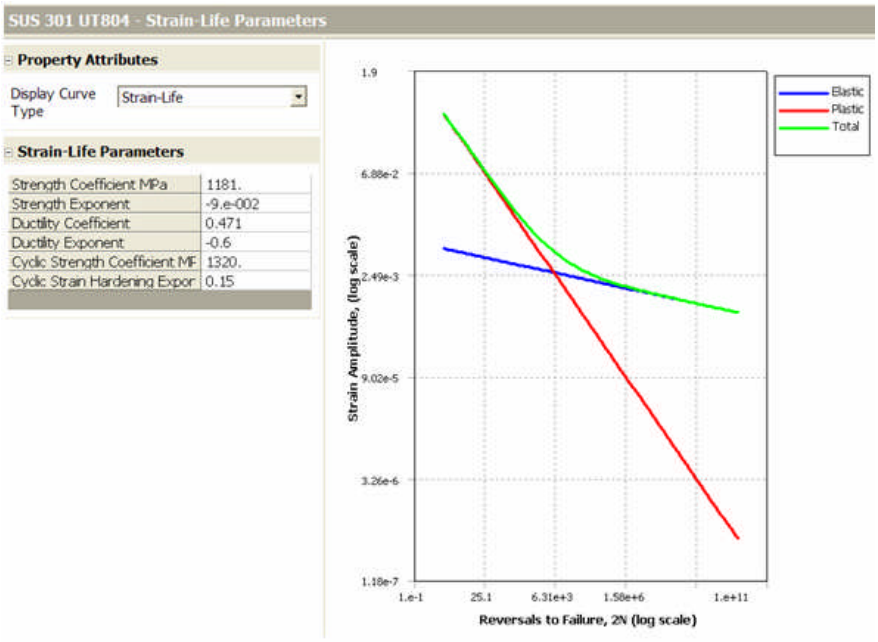

Strain- Life curve for SUS 301 804 MPa tensile strength

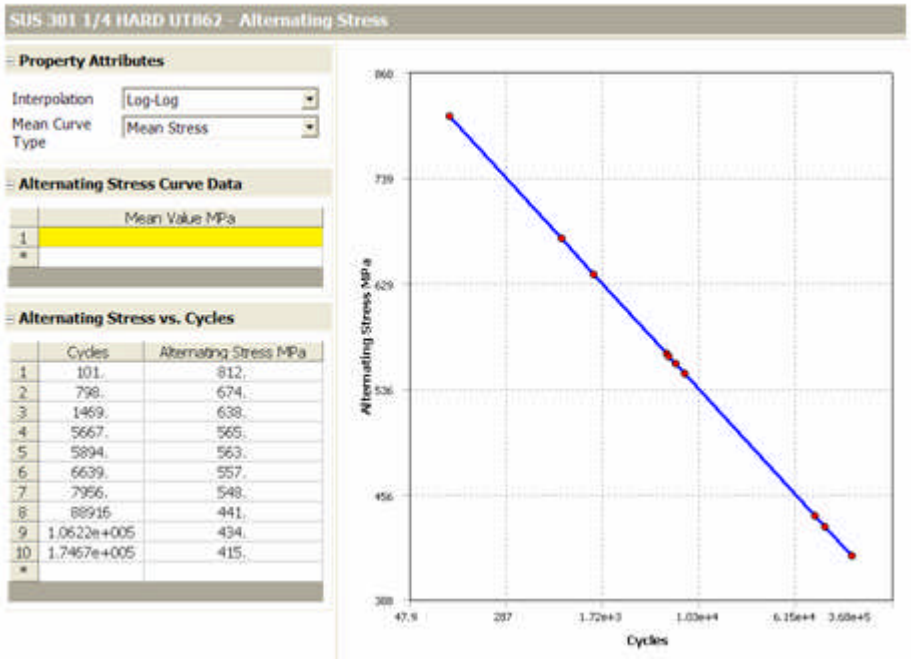

Figure 4.4.5: Stress- Life curve for SUS 301 1/4 cold-rolled

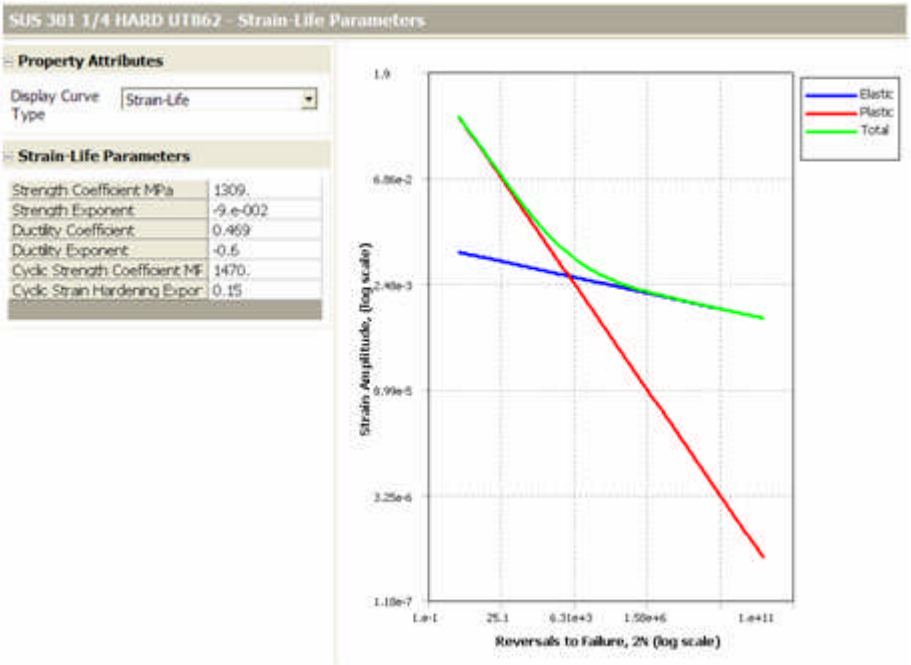

Figure 4.4.6: Strain- Life curve for SUS 301 1/4 cold-rolled

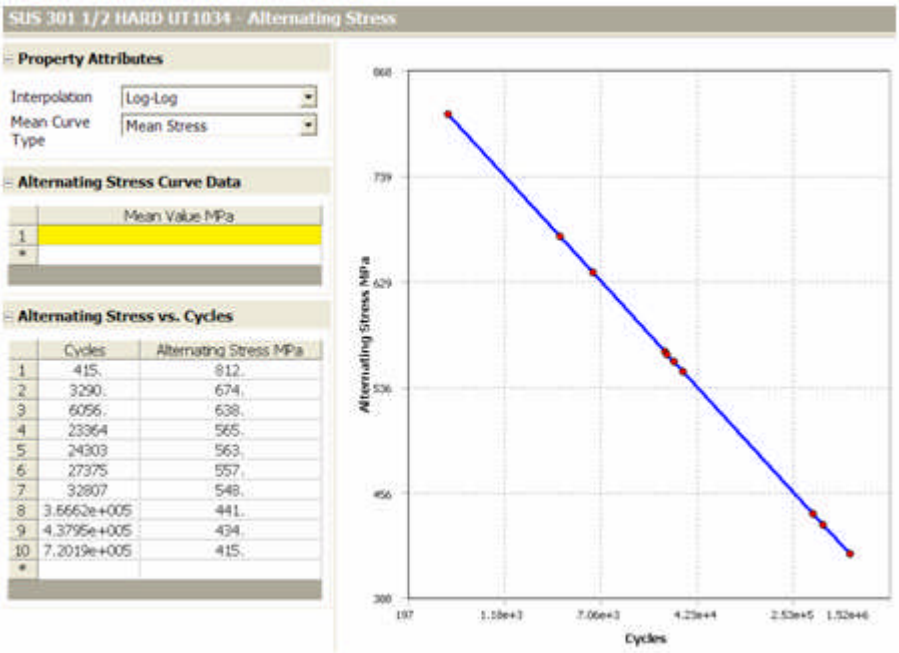

Figure 4.4.5: Stress- Life curve for SUS 301 1/2 cold-rolled

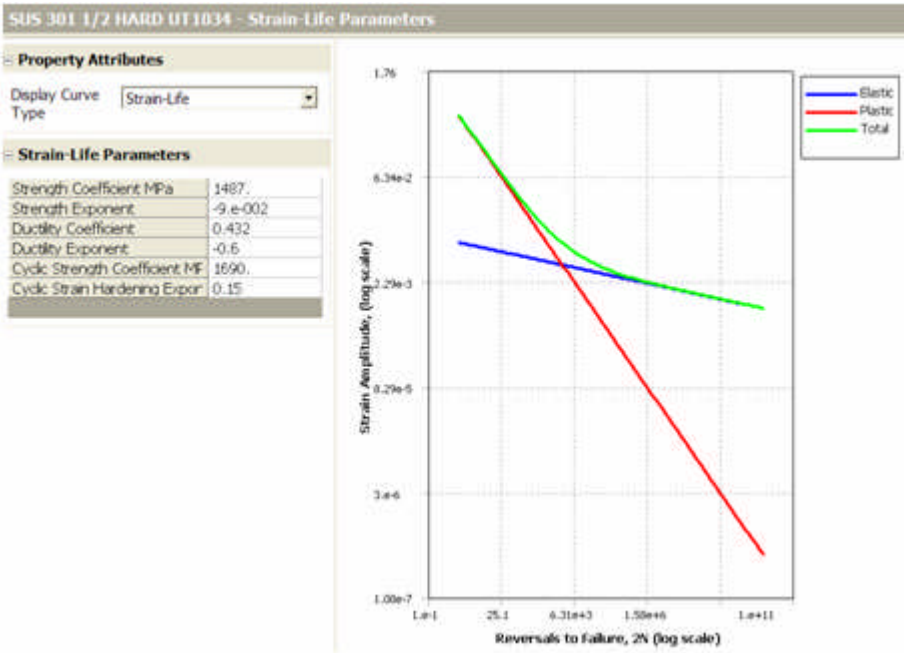

Figure 4.4.6: Strain- Life curve for SUS 301 1/2 cold-rolled